A Study of Refrigerant Void Fraction and Pressure Drop in Return Bends and Development of a New Two-Phase Experimental Apparatus

C. C. Tran, S. Gupta, T. A. Newell, and J. C. Chato

ACRC TR-167 June 2000

For additional information:

Air Conditioning and Refrigeration Center
University of Illinois
Mechanical & Industrial Engineering Dept.
1206 West Green Street
Urbana, IL 61801

(217) 333-3115

Prepared as part of ACRC Project 100
Refrigerant/Oil Mixtures in Horizontal Tubes and Flat Plate Evaporators
T. A. Newell and J. C. Chato, Principal Investigators

The Air Conditioning and Refrigeration Center was founded in 1988 with a grant from the estate of Richard W. Kritzer, the founder of Peerless of America Inc. A State of Illinois Technology Challenge Grant helped build the laboratory facilities. The ACRC receives continuing support from the Richard W. Kritzer Endowment and the National Science Foundation. The following organizations have also become sponsors of the Center.

Amana Refrigeration, Inc.
Arçelik A. S.
Brazeway, Inc.
Carrier Corporation
Copeland Corporation
DaimlerChrysler Corporation
Delphi Harrison Thermal Systems
Frigidaire Company
General Electric Company
General Motors Corporation
Hill PHOENIX
Honeywell, Inc.
Hussmann Corporation
Hydro Aluminum Adrian, Inc.
Indiana Tube Corporation
Invensys Climate Controls
Lennox International, Inc.
Modine Manufacturing Co.
Parker Hannifin Corporation
Peerless of America, Inc.
The Trane Company
Thermo King Corporation
Valeo, Inc.
Visteon Automotive Systems
Whirlpool Corporation
Wolverine Tube, Inc.
York International, Inc.

For additional information:

Air Conditioning & Refrigeration Center
Mechanical & Industrial Engineering Dept.
University of Illinois
1206 West Green Street
Urbana, IL 61801

217 333 3115

Abstract

A STUDY OF REFRIGERANT VOID FRACTION AND PRESSURE DROP IN RETURN BENDS
AND
DEVELOPMENT OF A NEW TWO-PHASE EXPERIMENTAL APPARATUS

Calvin Cuong Tran
Department of Mechanical and Industrial Engineering
University of Illinois at Urbana-Champaign, 1998
Ty Newell and John C. Chato, Advisors

Void fractions and pressure drops were measured for R134a and R410A for a return bend test section consisting of three return bends of tube diameter 8.28 mm (0.326") and center-to-center distances of 25.4 mm (1.00"). The test matrix included mass fluxes from 65 kg/m^2 s to 440 kg/m^2 s (48 – 324 klb_m/ft^2-hr) and test section qualities from 5% to 70% with an inlet temperature of 5°C (41°F). Three orientations consisting of vertically upward, horizontal, and vertically downward were tested.

Negligible effects on void fraction were measured relative to straight tubes. Pressure drop data showed some trends due to changes in quality, mass flux, refrigerant, and orientation. The pressure drop increased with both quality and mass flux. The lower pressure refrigerant had a larger pressure drop. Downflow to upflow orientations resulted in increasing pressure drop.

A new apparatus for studies in evaporation was constructed at the University of Illinois at Urbana-Champaign. Details on system structure, components, and operation are given.

Table of Contents

List of Tables

List of Figures

Nomenclature

C_d	Center-to-Center Distance in Bend (m)
D	Inside Diameter in Bend (m)
f_g	Friction Factor [Geary]
G	Mass Flux (kg/m^2 s)
g	Gravitational Constant = 9.81 m/s^2
h	Enthalpy
l	Bend Length [Geary]
$\dot{m}$	Mass Flow Rate (kg/s)
P	Pressure (kPa)
$\dot{Q}$	Power (W)
v	Specific Volume
x	Quality
z	Distance

Greek Symbols

α	Void Fraction
δ	Bend Characterization Parameter = $\sqrt{D/C_d}$
μ	Viscosity (kg/m s)
ρ	Density (kg/m^3)

Dimensionless Parameters

ε	Resistance Factor [Pierre, Christoffersen]
Fr	Froude Number
Ft	Modified Froude Rate [Graham]
Φ^2	Multiplier [Souza, Jung and Radermacher]
Re	Reynolds Number
X, Xtt	Lockhart-Martinelli Parameter

Subsripts

ave	Average
b	Bend [Pierre, Christoffersen, Geary]
f	Frictional [Pierre, Christoffersen]
l	Liquid
lo	Liquid Only
sub	Subcooled
t	Turning [Pierre]
tp	Two Phase
v	Vapor

Chapter 1

Introduction

With the significance of multi-phase flows in refrigeration and air-conditioning systems, void fraction has been found to be an important parameter in characterizing the flows. Void fraction allows the prediction of refrigerant charge in systems. Also, void fraction aids in the determination of other factors such as pressure drop and heat transfer.

Although many studies were performed to determine the void fraction in smooth tubes, no studies were performed to predict the void fraction in systems with return bends, as is typical in cooling systems. Chapter 2 examines these effects of the return bends on the void fraction as well as determines the effects of these bends on pressure drop. Although a few studies were performed on return bend two-phase pressure drop, these studies have not examined the pressure drop in return bends using R134a and R410A with a bend diameter and center-to-center distance of that typical in wall air-conditioning systems.

Chapter 3 discusses the developments of a new experimental apparatus used for these tests. The new system will permit testing of a wider range of conditions and allow for a more complete picture of void fraction, pressure drop, and heat transfer in both pure refrigerants as well as oil/refrigerant mixtures. Chapter 4 will conclude with the major findings of the return bend study as well as some final statements on the new experimental apparatus.

Chapter 2

Return Bend Effects On Pressure Drop and Void Fraction

2.1. Introduction

Void fraction and pressure drop in an air-conditioning or refrigeration system are important design factors. The void fraction allows designers of reduced-charge systems to minimize refrigerant charge within the refrigerant system as well as better predict the heat transfer characteristics of a system. Studies were performed by Wilson [1998] and others to determine the void fraction in straight tubes; however, refrigerant void fraction in return bends appears to have not been studied.

Pressure drops within an air conditioning or refrigeration system create inefficiencies for the compressor and cause more work due to increasing the high-to-low side pressure difference. Pressure drop in return bends was studied by Pierre [1964], Geary [1975], and Christoffersen [1993]. This paper will compare the current data with the models by Pierre, Geary, and Christoffersen, as well as discuss the discrepancies in the results. Trends due to quality, mass flux, refrigerant, and orientation will also be presented.

2.2. Background

Considerable work was completed for correlations in pressure drop for straight tubes. Significantly less work on pressure drop was performed on return bend fittings, however. Three pressure drop correlations for pressure drops in return bends were found and will be discussed.

Two pressure drop correlations for straight tubes are used to compare with the data from this experiment. These correlations are based on the separated flow model developed by Lockhart and Martinelli [1949]. Lockhart and Martinelli postulated that the pressure drop of a two-phase flow could be correlated to the pressure drop due to pure liquid flow and pure vapor flow. The Lockhart-Martinelli parameter, X, was developed and is given as follows:

$$X = \left[\frac{\left(\frac{\Delta P}{\Delta z} \right)_l}{\left(\frac{\Delta P}{\Delta z} \right)_v} \right]^{0.5} \tag{2.1}$$

Assuming both phases of flows are turbulent, the Lockhart-Martinelli parameter can be defined as:

$$X_{tt} = \left(\frac{1 - x_{ave}}{x_{ave}} \right)^{0.9} \left(\frac{\rho_v}{\rho_l} \right)^{0.5} \left(\frac{\mu_l}{\mu_v} \right)^{0.1} \tag{2.2}$$

Relations for multipliers to find two-phase pressure drops use Xtt. The relation is:

$$\Phi^2 = \frac{(\Delta P)_{tp}}{(\Delta P)_{lo}} \tag{2.3}$$

Jung and Radermacher [1989] developed a two-phase multiplier to be:

$$\Phi^2 = 12.82 X_{tt}^{-1.47} (1 - x)^{1.8} \tag{2.4}$$

This multiplier actually takes into account both the frictional and acceleration pressure drops. The acceleration pressure drop was less than 10% of the total pressure drop for the conditions tested by Jung and Radermacher as indicated by Soumerai [1987]. Souza [1993] developed the following pressure drop correlation:

$$\Phi^2 = (1.376 + c_1 X_{tt}^{-c_2})(1-x)^{1.75} \tag{2.5}$$

For $0 < Fr_l \leq 0.7$

$c_1 = 4.172 + 5.480Fr_l - 1.564Fr_l^2$

$c_2 = 1.773 - 0.169Fr_l$

For $Fr_l > 0.7$

$c_1 = 7.242$

$c_2 = 1.655$

where Fr_l is defined as:

$$Fr_l = \frac{G^2}{\rho_l^2 gD} \tag{2.6}$$

Souza separated the friction and acceleration pressure drops for the multiplier. A Froude number effect was also included in order to take the flow regime into account.

For the return bends, three correlations for pressure drop are examined. These models are based on two classes. The first class decomposes the pressure drop due to the bends into one part that turns the flow and another part that resists the flow due to friction as seen in the following equation:

$$\Delta P_b = \Delta P_t + \Delta P_f \tag{2.7}$$

Pierre [1964] developed a resistance factor, ε, that was used to calculate the turning of the flows. This equation is given as:

$$\varepsilon = \frac{2\Delta P_t}{G^2 v_{ave}} \tag{2.8}$$

The resistance factor was found to be within a range of 0.8 to 1.0 when oil was not present. Christoffersen [1993] felt the constant resistance factor was valid for single phase flows; however, due to the viscous effects, secondary flows, and separation, Christoffersen created a correlation that allowed for a varying resistance factor. The correlation is:

$$\frac{2\varepsilon}{\delta \mathrm{Re}_l} = C_1 X_{tt}^{C_2} \tag{2.9}$$

where C_1 equals $6.93*10^{-5}$ and C_2 equals –0.712. Geary [1975] created a correlation for the entire pressure drop of the bend without separating the turning and frictional pressure drops. Geary determined a friction factor with the form:

$$f_g = \frac{5.58*10^{-6}\,\mathrm{Re}_v^{0.5}}{\exp(0.215C_d / D)x^{1.25}} \tag{2.10}$$

The constant $5.58*10^{-6}$ in the equation has dimensions of ft^2/in^2. This constant should be made dimensionless and then used to calculate the pressure drop in the bend using the following equation:

$$\Delta P_b = f_g \frac{l}{D}\frac{G_v^2}{2\rho_v} \tag{2.11}$$

2.3. Experimental Design

The experimental apparatus for evaporation was used to condition the mass flux, quality, and temperature at the inlet of the test section. Mass flux ranges from 65 to 440 kg/(m^2 s) and qualities from 5 to 70% were obtained. The inlet temperature was 5° C. Adiabatic conditions were tested. Conditions were monitored using a Hewlett Packard data acquisition system. A schematic of the loop is shown in Figure 2.1.

Subcooled R134a or R410A refrigerant was driven through the loop using a pump. The pump was used to control the mass flux of the refrigerant going through the loop. The refrigerant was forced into a pre-heater as seen in Figure 2.1., where electrical heater strips were used to add energy to the refrigerant and change the quality to a specified value. This conditioned refrigerant proceeded into the return bend test section

and was subcooled at a condenser downstream of the test section. The return bend test section was oriented in three ways so that the refrigerant flowed horizontally, vertically downward, and vertically upward in the return bends. A schematic of the test section is shown in Figure 2.2.

After the refrigerant had reached and remained at constant conditions for at least 30s, the pressure transducer valves on the test section were first closed, followed by the valves for the test section. After the test section had been closed off, an evacuated receiver tank was connected to the test section void fraction tap. The refrigerant was discharged into the tank and the mass of the refrigerant was determined. The final vapor mass remaining in the test section was calculated from the temperature and pressure conditions. With the total mass, test section volume, and test section temperature/pressure, the void fraction was determined. A sample Engineering Equation Solver (EES) code for calculating this can be found in Appendix A. The test section pressure drop was averaged from a set of readings taken from the differential pressure transducer while the loop was running under steady state conditions and before the test section was closed off. Additional information on the operation of the test loop as well as the void fraction collection technique is detailed in Wilson [1998].

2.4. Results

The effects of return bends on both the void fraction and pressure drop are observed and analyzed. Uncertainties are also presented.

2.4.1. Void Fraction

The void fraction was obtained using the procedure mentioned in Section 2.3. Previous testing was performed to find the void fraction in straight tubes. From the study at the University of Illinois, the void fraction was found to be a function of the Lockhart-Martinelli parameter (Xtt) and the Froude rate (Ft) as given in Graham [1999]. This relation is:

$$\alpha = \left[1 + \frac{1}{Ft} + X_{tt}\right]^{-0.321} \tag{2.12}$$

where Ft is defined as

$$Ft = \left[\frac{x^3 G^2}{\rho_v^2 g D(1-x)}\right]^{\frac{1}{2}} \tag{2.13}$$

Void fractions in straight tubes were compared with the void fractions found for the return bend test section. As seen from Figure 2.3., the effects on void fraction due to the return bend under evaporative conditions appears to be small. This may not be true in the condenser, however, because the higher temperatures under condenser conditions lead to higher vapor densities. At a given mass flux, increased vapor density reduces the vapor velocity, which causes less shearing of the liquid film on the tube wall, resulting in more liquid mass in the tube. A similar study under condenser conditions may lead to substantially different results.

2.4.1.1. Void Fraction Uncertainty

The uncertainty for the void fraction was calculated after determining the bias and precision errors associated with the measurements. These errors in making the measurements are given in Table 2.1.

Table 2.1. Bias and Precision Errors

Measurement	Bias Error	Precision Error	Total Error
Thermocouple	±1° C	±0.14° C	±1° C
Pressure Transducer (Absolute)	±0.75 %	±0.70 %	±1.0 %
Mass Scale	±1.0E-05 kg	±4.5E-04 kg	±4.5E-04 kg
Volume	±7.2-07 m^3	±2.6E-05 m^3	±2.6E-05 m^3
Calipers	±0.000254 m	±0.0001 m	±0.00027 m

The bias errors, $B_{\bar{x}}$, were the systematic errors due to the instrument calibration or data reduction. Most of these errors were due to the instrument calibration themselves. In the case of the volume measurement, however, the other errors were entered into EES and the error calculated using the Uncertainty Propagation feature within EES that propagates the errors in a calculation. The precision errors, $P_{\bar{x}}$, were the random errors affecting the repeatability of a certain measurement. The precision errors were calculated using Equation 2.14.

$$P_{\bar{x}} = \frac{tS_x}{\sqrt{N}} \tag{2.14}$$

where t is a value from the t distribution with a confidence level of 0.95, S_x is the standard deviation of the measurements, and N is the number of measurements. Once again, the precision error for the volume was calculated using EES. The total error, $U_{\bar{x}}$, was then calculated using Equation 2.15.

$$U_{\bar{x}} = (B_{\bar{x}}^2 + P_{\bar{x}}^2)^{\frac{1}{2}} \tag{2.15}$$

The total error for void fraction was determined using EES and the errors given in Table 2.1. The result of this calculation for void fraction is given in Figure 2.4. These are representative errors found for the void fraction in the horizontal orientation.

2.4.2. Pressure Drop

Pressure drop was measured across the test section at the pressure taps as seen in Figure 2.2. The accuracy of the transducer is ±0.25% full scale. This gave the test section pressure drops as seen in Figure 2.5. and Figure 2.6.

Figure 2.5. shows that the pressure drop increases with quality. At higher qualities there is a much greater mass of vapor than at lower qualities. The quality increases cause the vapor velocity to increase, creating a greater frictional pressure drop. This greater vapor velocity is also the reason why the pressure drop for a lower pressure refrigerant is higher. Figure 2.5. also shows a slight trend of increasing pressure drop as the test section is oriented from downflow to upflow orientations. This small effect is most likely due to gravity.

The pressure drop is also very dependent on the mass flux as seen in Figure 2.6. As the mass flux increases, the pressure drop also increases. At a given quality, with an increasing mass flux, there is considerable variation in the increase in the vapor and liquid velocities. This results in greater frictional pressure drop as the difference between the vapor and liquid velocities increases.

The pressure drops for the return bends were found by subtracting the estimated pressure drop due to the straight sections of tubing. The Souza correlation as well as the Jung and Radermacher correlation for straight, horizontal tubes were examined. Both correlations generated similar results for straight tube pressure drop. The Souza correlation was chosen for comparison purposes and accounts for approximately 20 to 40% of the test section pressure drop. The resulting pressure drop per return bend is shown in Figure 2.7.

2.4.2.1. Pressure Drop Uncertainty

The accuracy of the pressure drop data is dependent on the Sensotec differential pressure transducer. This transducer has a bias error of 0.25% full scale. The total errors were calculated for each data point. These errors ranged from 2 to 40% for the test section, with the average for R134a being 18% and the average for R410A being 12%. The errors for the return bends ranged from 10 to 50% with the average error for R134a being 25% and the average for R410A being 22%. There was considerable fluctuation in the pressure readings. This fluctuation was mostly due to the transition in flow regimes since very minute fluctuations were observed under no flow conditions.

2.5. Discussion

The pressure drop data was compared with other pressure drop correlations developed for return bends. Three correlations were described in the background section. As seen from Figure 2.8. and Figure 2.9., the test section and return bend pressure drops from this study were significantly higher than that predicted by the Christoffersen, Pierre, and Geary correlations. This may be due to several reasons. First, from the construction of the test section, the straight sections of tubing were inserted into the return bend tubes rather than butted or coupled together. This abrupt change in diameter from the return bends to the straight sections may have increased the return bend pressure drop. The ratio of the bend diameter to the center-to-center distance may have an effect on pressure drop also. The increase in pressure drop may have been due to the tighter turning return bends in this study than that seen in the Christoffersen and Pierre studies, although the

ratios studied by Geary do cover bends that turn even tighter. The bend diameters and center-to-center distances as well as the ratios covered in the studies are presented in Table 2.2.

Table 2.2. Comparison of Geometric Data in the Return Bend Studies

Study	d (mm)	C_d (mm)	d/C_d
Present Study	8.28	25.4	0.326
Christoffersen	8.00	76.2	0.105
	11.0	76.2	0.144
	8.00	47.5	0.168
Pierre	10.9	75.0	0.145
	10.9	38.0	0.287
	10.9	75.0	0.145
Geary	11.0	25.6	0.432
	11.4	31.8	0.358
	11.6	35.1	0.332
	11.4	43.2	0.263
	10.6	50.4	0.211
	11.4	50.8	0.224
	11.4	63.5	0.180
	11.4	74.5	0.153

Additional error was due to the sensing of the equipment. The differential pressure transducer has an accuracy of ±0.25% full scale. The thermocouples had uncertainties of ±1° C. The absolute pressure transducers had uncertainties of ±0.75% full scale. These errors as well as the total error of ±0.45 g from the mass scale contributed to the overall inaccuracies in measurement. Error resulted from using the Souza correlation as well. The reported accuracy of the correlation is ±10%.

2.6. Conclusion

Void fraction and pressure drop data are presented here for return bends for two refrigerants over a range of mass flux and quality conditions. Return bend results from

this investigation appear to have minimal effect on the void fraction in evaporative conditions. The return bends did seem to have considerable effect on the pressure drop, however. An increase in pressure drop occurred with increasing quality. Also, the lower pressure refrigerant had a higher pressure drop. Some gravitational effects due to orientation were seen to effect the pressure drop. The return bend pressure drops measured did not correlate well with existing correlations, however, the primary differences may be due to the connection between the return bend and the straight tubes and due to the size of the return bend relative to those examined in the development of the correlations. Further study of the return bends is recommended.

2.7. Figures

Several schematics and plots are included here concerning the return bend test apparatus, test section, and data. Additional plots and the raw data are located in Appendix B.

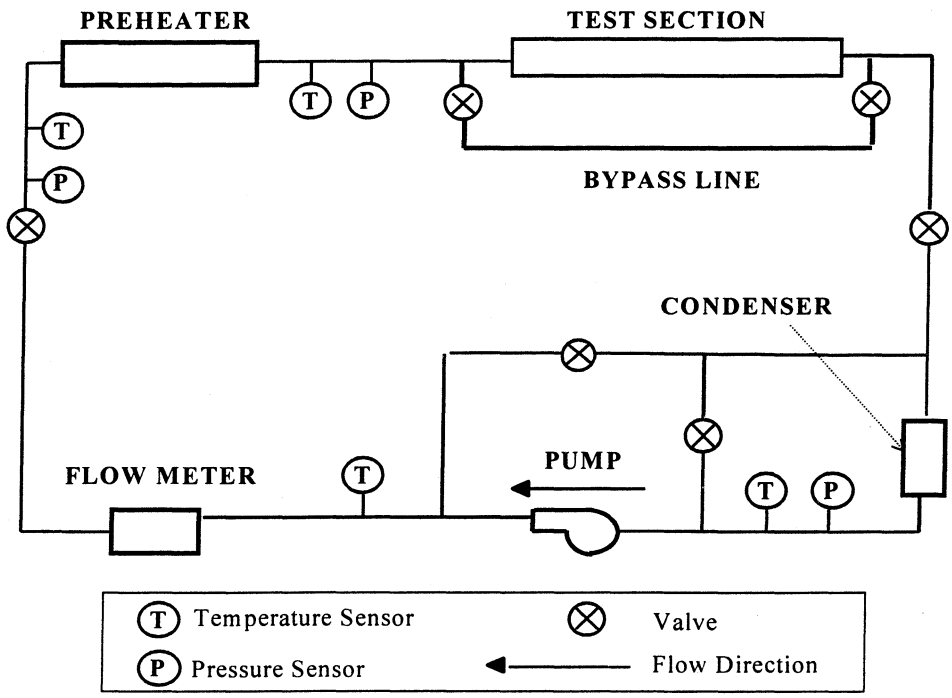

Figure 2.1. Test Section Schematic

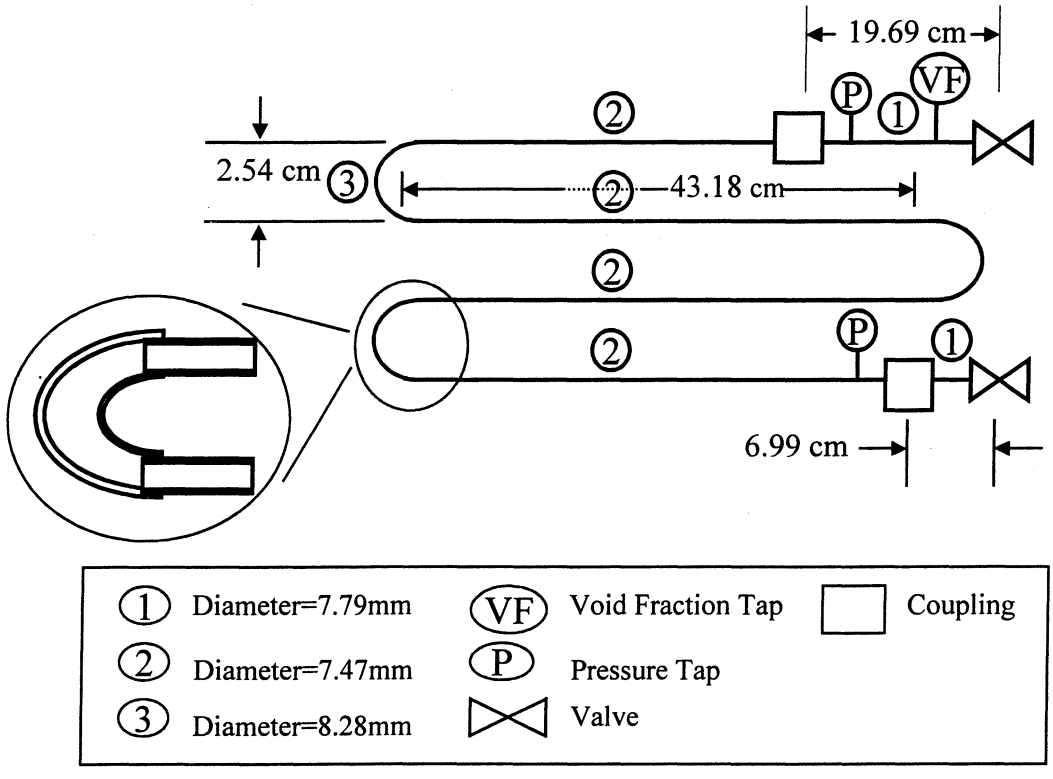

Figure 2.2. Return Bend Diagram

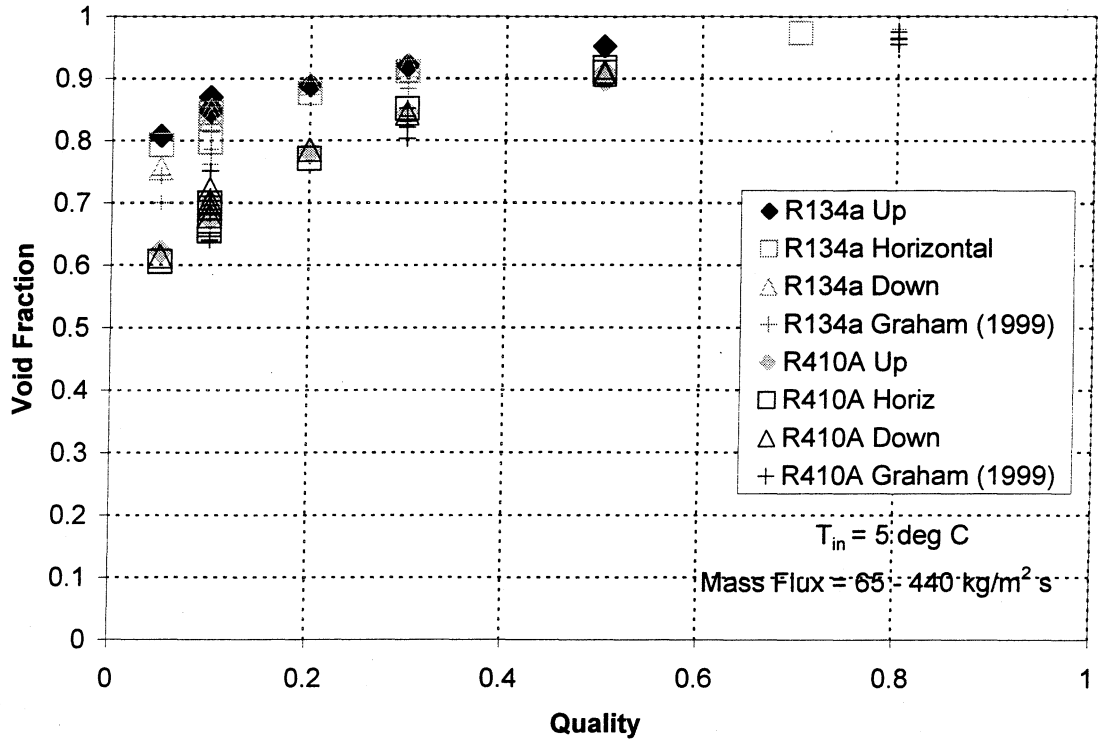

Figure 2.3. Test Section Void Fraction vs. Quality

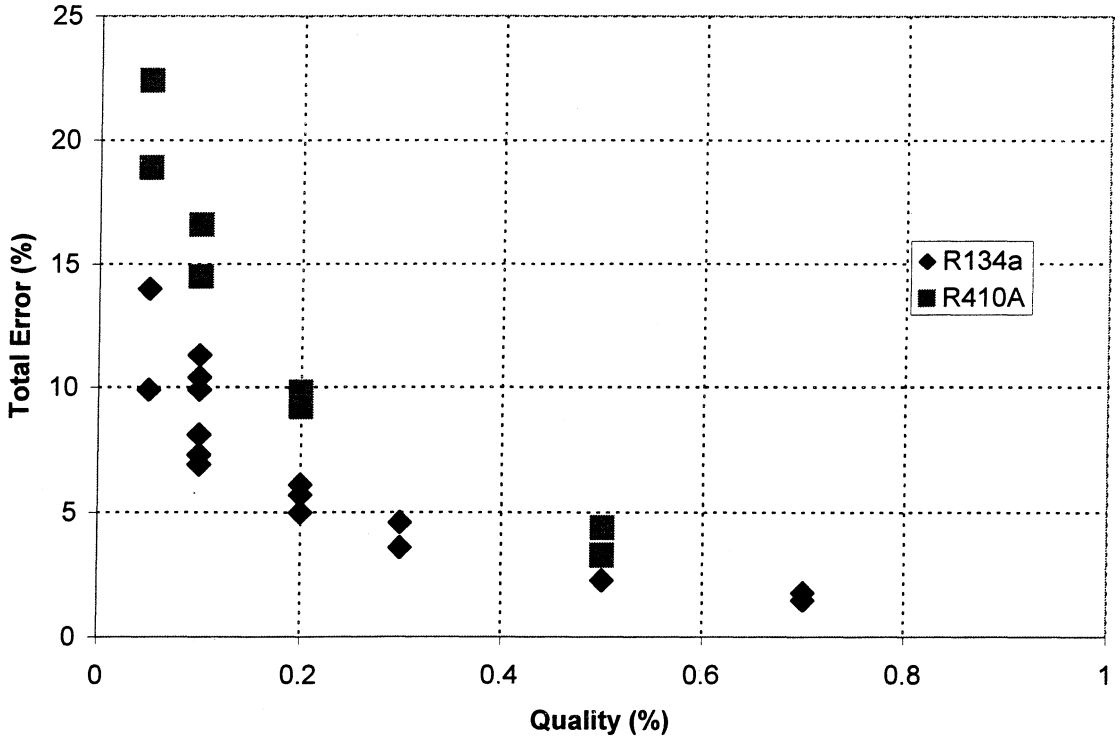

Figure 2.4. Representative Void Fraction Total Error of Test Section in the Horizontal Position vs. Quality

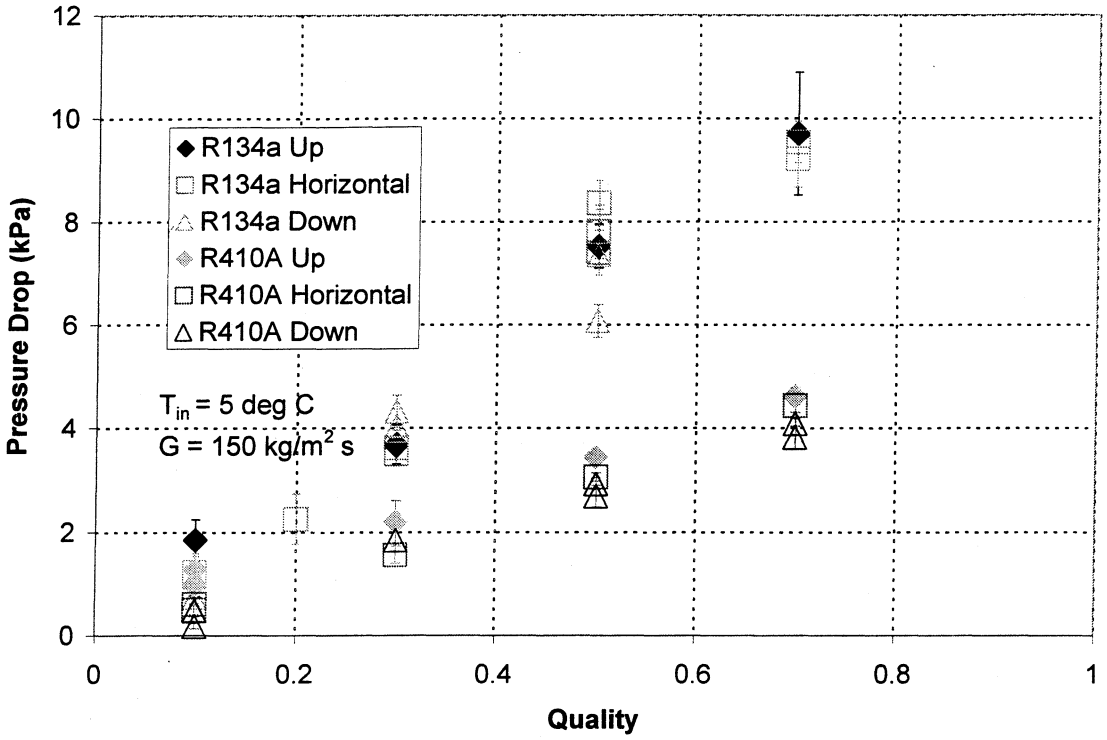

Figure 2.5. Test Section Pressure Drop vs. Quality

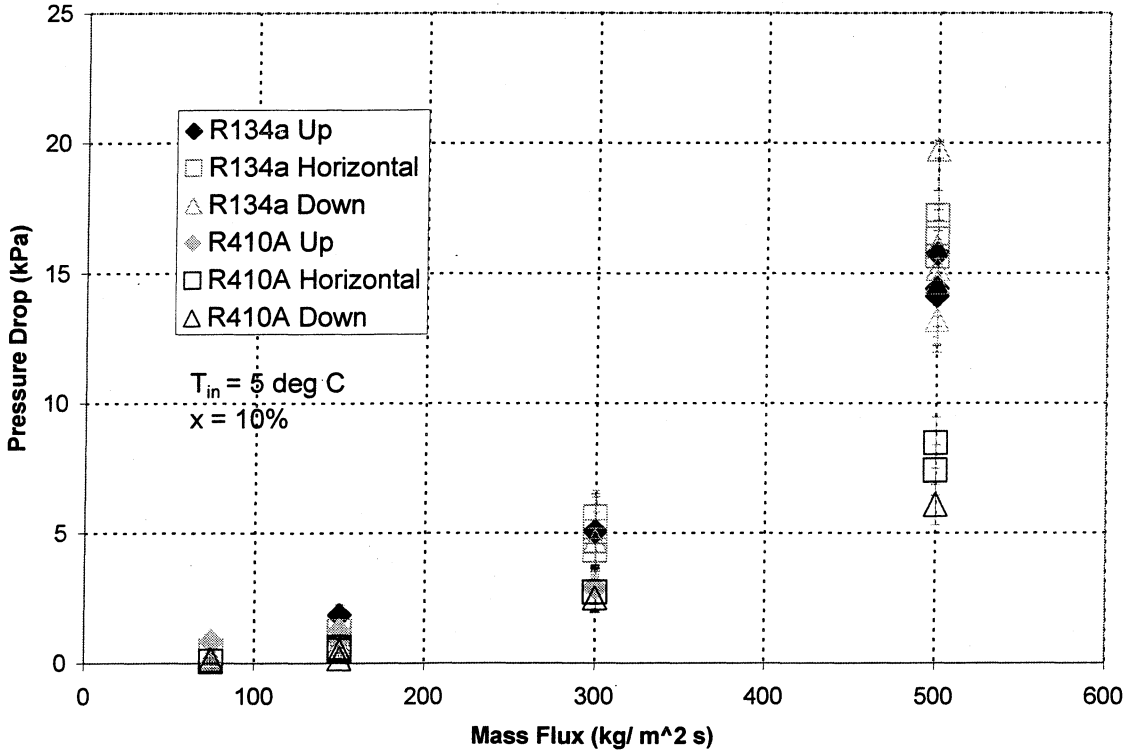

Figure 2.6. Test Section Pressure Drop vs. Mass Flux

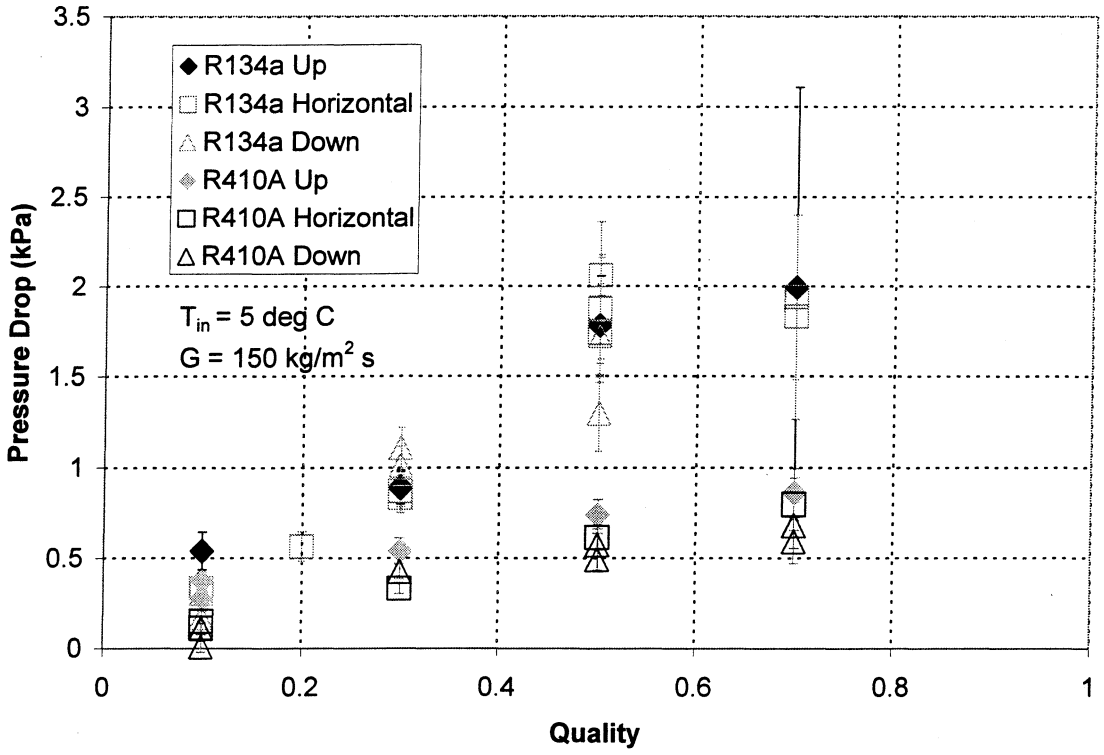

Figure 2.7. Return Bend Pressure Drop vs. Quality

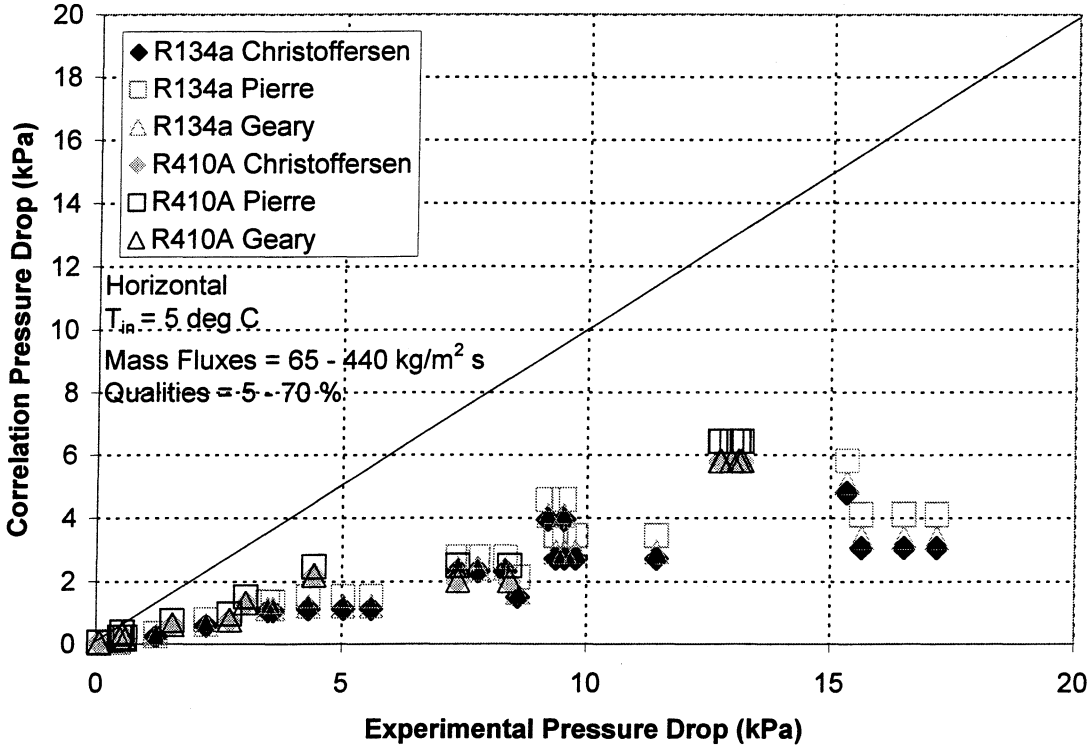

Figure 2.8. Comparison of Experimental and Correlation Pressure Drops in the Test Section

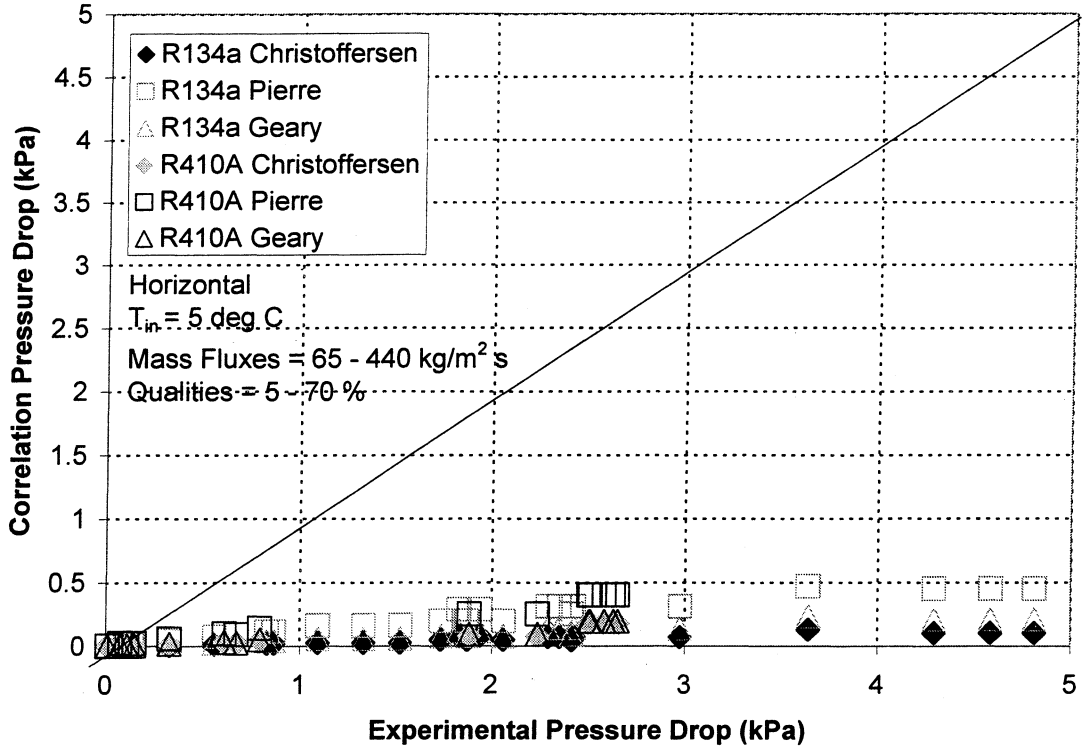

Figure 2.9. Comparison of Experimental and Correlation Pressure Drops in the Return Bend

2.8. References

Christoffersen, B. R., J. C. Chato, J. P. Wattelet, and A. L. de Souza. 1993. Heat Transfer and Flow Characteristics of R-22, R-32/R-125, and R-134a in Smooth and Micro-Fin Tubes. M.S. Thesis, Department of Mechanical and Industrial Engineering, University of Illinois, Urbana.

Geary, D. F. 1975. Return Bend Pressure Drop in Refrigeration Systems. *ASHRAE Transactions*, 81: 250-265.

Graham, D. M., H. R. Kopke, M. J. Wilson, D. A. Yashar, J. C. Chato, and T. A. Newell. 1999. An Investigation of Void Fraction in the Stratified/Annular Flow Regions in Smooth, Horizontal Tubes. ACRC TR-144, Air Conditioning and Refrigeration Center, University of Illinois, Urbana.

Jung, D. S., and Radermacher. 1989. Prediction of Pressure Drop During Horizontal Annular Flow Boiling of Pure and Mixed Refrigerants. *International Journal of Heat and Mass Transfer*, 32: 2435-2446.

Lockhart, R. W. and R. C. Martinelli. 1949. Proposed Correlation of Data for Isothermal Two-Phase, Two-Component Flow in Pipes. *Chemical Engineering Progress*, 45: 39-48.

Pierre, B. 1964. Flow Resistance with Boiling Refrigerants–Part II. *ASHRAE Journal*, 6(10) 73-77.

Soumerai, H. 1987. Practical Thermodynamic Tools for Heat Exchanger Design Engineers. Wiley. New York.

Souza, A. L., J. C. Chato, J. P., Wattelet, and B. Christoffersen. 1993. Pressure Drop During Two-Phase Flow of Pure Refrigerants and Refrigerant-Oil Mixtures in Horizontal Smooth Tubes. *Heat Transfer with Alternate Refrigerants* (ASME), 243: 35-41.

Wilson, M. J., T. A. Newell, and J. C. Chato. 1998. Experimental Investigation of Void Fraction During Horizontal Flow in Larger Diameter Refrigeration Applications. ACRC TR-140, Air Conditioning and Refrigeration Center, University of Illinois, Urbana.

Chapter 3

Experimental Facilities and Measurement Devices

A new evaporation test facility at the University of Illinois at Urbana-Champaign was constructed and completed in the Spring of 2000. The purpose of this chapter is to describe the apparatus, instrumentation, and data acquisition system used. An overview of the apparatus will be given followed by an examination of the main components in the experimental loop. The new Hewlett Packard data acquisition system and the HP VEE data acquisition software will then be described. After that, details on the instrumentation that will be connected to the data acquisition system will be given. Procedures on the operation of the new loop will also be presented.

3.1. Experimental Test Facility

The experimental facility consists of a refrigerant loop, a chiller system, and a test section. In the following sections each part of the test facility will be described.

3.1.1. Refrigerant Loop

The purpose of the refrigerant loop is to reproduce the evaporative conditions typical in air-conditioning and refrigeration applications. The conditions controlled are the test section inlet temperature, mass flux, inlet quality, and heat flux.

A schematic of the refrigerant loop appears in Figure 3.1. Two refrigerant lines, the liquid and the vapor lines, comprise the loop. At the center of the loop is a separator

tank that combines the refrigerant at saturated state. From here, a pump drives liquid through the liquid line and a compressor forces vapor through the vapor line.

In the liquid line, saturated liquid is drawn from the bottom of the separator tank. This tank is partially submerged in an ice water slurry. This slurry condenses the refrigerant to approximately 3°C and helps to ensure liquid refrigerant is present at the bottom of the separator tank. The liquid is then drawn from the bottom of this tank by a variable speed gear pump, which forces the liquid refrigerant to flow through the loop. The actual mass flow rate of this refrigerant is set by either adjusting the speed of the pump or adjusting a needle valve that is on the bypass line. This liquid mass flow rate is measured using a Coriolis-type mass flow meter manufactured by Micro-Motion®. This meter is just downstream of the pump. Next the refrigerant flows through a pre-heater section which conditions the flow to the desired inlet quality. Physically, the pre-heater consists of three 1.8 meter passes of 3/8" (0.95 cm) outer diameter copper tube in a serpentine shape. The outside of the tube is wrapped with eight Minco® electrical heating strips of various resistances. Six of the strips are controlled by three switches and deliver fixed amounts of power to the pre-heater. A 115 V variac allows incremental amounts of power to be delivered to the other two strips. From here the refrigerant is conditioned to flow into the test section as in the case of the original loop.

The Corken oil-free compressor drives the vapor in the loop. The compressor forces the refrigerant vapor in the vapor line to flow from the upper portion of the separator tank to a 13.6 kg (30 lb) refrigerant tank. This tank helps to dampen the compressor oscillations. The compression of the vapor causes the refrigerant temperature to increase. Therefore, a heat exchanger was incorporated to remove some of the heat,

but still leave the vapor outside of the saturation dome. This vapor then travels to another tank that also dampens the oscillations caused by the compressor. The flow rate is sensed by a Coriolis-type mass flow meter manufactured by Micro-Motion®. The rate is controlled using a needle valve that is located in the vapor line. A bypass line is also present with a needle valve to further control the flow of the vapor. This vapor then mixes with the refrigerant from the liquid line creating a saturated condition at 5°C with a certain mixture quality and mass flux. This mixture then enters the test section.

When the test section is closed for void fraction measurements a test section bypass valve is opened to allow the refrigerant to continue circulating. This refrigerant returning from the test section bypass or test section then enters a heat exchanger and then proceeds to the saturated separator tank.

3.1.2. Chiller

The chiller system helps remove heat from the refrigerant loop using heat exchangers located in the experimental loop. One heat exchanger is located downstream of the compressor and the other is located downstream of the test section. These heat exchangers remove the heat added from the compressor, pre-heater, as well as the test section heaters.

The chiller system is a propylene glycol-water based system. It is a cascading system comprised of a propylene glycol and water loop, and a R22 refrigeration loop that is connected to the municipal water supply. A schematic of the chiller is seen in Figure 3.2.

The R22 refrigeration loop uses the compressor from a 1.5 ton (5.3 kW) air-conditioning system. Heat from the experimental loop is drawn into the Standard Refrigeration tube-in-tube evaporator (TNT-150) via the propylene glycol, evaporating the R22 and cooling the glycol. The compressor then drives this R22 vapor to the Standard Refrigeration condenser (TNT-150) to remove the heat from the chiller system using cold water. Cold water from the municipal water system enters the condenser of the chiller around 15° C at a rate modified using a needle valve. The liquid R22 from the condenser is then forced through a liquid line drier-filter, a sight glass and a needle valve back to the evaporator.

The propylene glycol loop is driven using a Milton Roy pump (GPPS-45H-1). The pump pushes cold glycol from the R22 evaporator to the plate heat exchangers located on the experimental loop. These heat exchangers act as the evaporator for the glycol loop, removing heat from the test experimental loop.

3.1.3. Test Section

Many different test sections can be used for study under evaporative conditions. Common test section types include straight cylindrical smooth and grooved tubes, flat plate evaporators, return bend test sections, and others. The test sections may contain spring lock connectors at the ends to allow for quick disconnect. This allows for a wider range of tests including void fraction tests with oil and refrigerant mixtures where oil holdup information may be desired.

As seen in Figure 3.1., the test apparatus contains two areas for test sections. This allows for faster data collection. As one flow condition is met, two test sections can be in

place for consecutive testing. It is also possible to perform tests on test sections of various lengths. Since the test section and refrigerant return line are constrained to the rest of the experimental apparatus by only one point on the return line, it is relatively easy to extend or shorten the allotted test section lengths.

3.2. Experimental Test Components

The main components of the loop will be discussed here.

3.2.1. Compressor

The compressor is used to drive vapor refrigerant in the vapor line to mix with the liquid refrigerant in the liquid line to obtain a certain quality. The Corken compressor (D91BJ4FBB) is an oil-free compressor. Special seals are used to seal the compression chamber from the oil in the crankcase. This allows pure refrigerant vapor to flow within the system and helps to ensure that none of the oil from the compressor enters the refrigerant loop. A motor that rotates at 181 rad/s (1730 rpm) spins a 9.53 cm (3.75 inch) driving wheel. The driving wheel is connected to the compressor flywheel by a belt. The flywheel has a diameter of 35.56 cm (14 inch) and an angular velocity of 47.33 rad/s (452 rpm). Thus, the piston displacement is 2070 cm^3/s (4.39 cfm). The compressor has a displacement volume of 290 cm^3. The minimum pressure required for the compressor is 20.7 kPa or 3 psi.

3.2.2. Heat Exchangers

Two Alfa Laval flat plate heat exchangers are used to remove the energy added to the system during operation. The heat exchanger after the test sections (CB14-28H S02) is rated for 1.25 tons (4.40 kW). Its dimensions are 20.7 x 7.7 x 7.2 cm. The heat exchanger after the compressor (CB22-10H H24E21) is rated for 0.75 tons (2.64 kW). The main purpose of this exchanger is to remove the heat added to the refrigerant due to the compression of gas. Since it is desired that this gas still remain in superheat, a smaller heat exchanger is necessary. Its dimensions are 31.8 x 8.1 x 3.1 cm. Software from SWEP Refrigeration Inc., SWEP version 96.11, was used to select the heat exchangers.

3.2.3. Pre-heater

The pre-heater section consists of three 1.8 meter passes of 3/8" (0.95 cm) outer diameter copper tube in a serpentine shape. A total of eight Minco® heater strips are used to condition the liquid refrigerant. Six of the heater strips (HK5373R66.5L12D) have 220 V across the strips and have resistances of 66.5 Ω. Three switches control these six strips. The first switch controls one heater strip, the second controls two and the third controls three. This leads to 730, 1460, and 2190 W for the three switches, respectively. The final two heater strips (HK5348R36.8L12D) have 110 V across the strips and resistances of 36.8Ω. These heater strips are connected to a variac controller. This allows energy from 0 to 660 W to be added to the system.

3.2.4. Pump

The Cole Parmer gear pump (7144-04) forces the liquid refrigerant through the experimental loop at mass fluxes typically ranging from 75 to 500 kg/m^2 s. With the rotational speed of the pump from 180 to 3600 rpm, the three-geared pump head (N-07003-04) is capable of volumetric flow rates up to 5 liters/min. A control driver (N-07144-04) is used to incrementally change this flow rate to the desired mass flow rates for testing.

3.2.5. Tanks

Three tanks are used in the new experimental loop. One AC&R, Inc. separator tank (S-5192) and two 13.6 kg (30 lb) refrigerator tanks are used. The separator tank has three ports. One port is at the bottom and two are located near the top of the tank. The tank is kept in an ice bath. This causes the saturated refrigerant entering the tank to condense and ensures liquid will be available for the pump while providing vapor near the top of the separator tank for the compressor. Both of the 30 lb refrigerator tanks are used to dampen the oscillations from the compressor.

3.3. Data Acquisition System

A new computerized data acquisition system is used to monitor and log data. In the original testing apparatus, a Macintosh II computer and a Strawberry Tree ™ data acquisition system were used. This system became unreliable due to age and caused considerable downtime, however, so it was replaced by a Hewlett Packard data

acquisition system comprised of a 75000 series B mainframe (E1300B) and a personal computer.

The 5.5 digit multimeter (E1326B) within the system can measure dc voltage, ac rms voltage, 2-wire and 4-wire resistances, as well as temperatures across three multiplexers. Temperatures are taken from the thermocouple multiplexer and dc voltage was taken for the 16-channel relay. The dc voltage was taken for four pressure transducers, three power transducers, and two flow meters. One of the pressure transducers and the three power transducers output dc voltage, however, the other sensors output a 4 – 20 mA current. The multimeter can read these output currents after a resistor is put across the terminals. A 250 ohm resistor is used for this purpose. The multimeter measures the dc voltage drop across the resistor.

As mentioned, three data acquisition multiplexer modules are used. Two 16-channel thermocouple relay multiplexer modules (E1347A) are for thermocouple readings. This allows the capability of 32 thermocouple readings to be taken concurrently. Type T thermocouples (Copper-Constantan) are used. The third module is a 16-channel relay (E1345A). It is used for voltage or current measurements for the other sensors. This module allows measurements from the pressure transducers, power transducers, and flow meters. The maximum voltage that can be applied across the terminals is 170 V dc or 120 V rms (170 V peak) for these multiplexers. A maximum current of 50 mA is allowed per channel.

The multiplexer consists of a component assembly and a terminal module. The component assembly is where the channel relay switches are located. The assembly is found within the mainframe. The terminal module, however, is where the field wiring

connects. Shielded wire is attached to the terminals of the terminal module making sure the wires were grounded. This grounding prevents the readings from drifting. This shielded wire then connects to jack panels (UJP-1-18-U, MJP-1-18-T). Various jacks (OST-U-M, SMP-T-M) are then connected to the ends of the sensor wires to allow quick disconnect. This is particularly useful for the test section thermocouples since the thermocouples must be disconnected in order to weigh the test section for void fraction measurements.

3.3.1. HP VEE Data Acquisition Software

HP VEE is a visual programming language used in data acquisition. Due to its visual nature, HP VEE is simple to use yet it is very powerful. Another major benefit of HP VEE is its interface with other programs. The ability to output data into Microsoft Excel has allowed for a more complete set of data with less time. Please see Appendix C for a sample of the command modules as well as some basic programming within HP VEE.

3.4. Instrumentation and Measurements

This section will discuss instruments and techniques used in measuring different parameters in the experiment. The parameters that were measured include temperature, pressure, mass flow rate, and power. Other quantities such as quality were calculated.

3.4.1. Temperature Measurements

Type T thermocouples (Copper-Constantan) are used for temperature measurements. The HP E1347A thermocouple multiplexer is thermocouple compensated and able to measure temperature upon specification of the thermocouple type. A reference thermistor is located on the multiplexer. This removes the need for an ice bath reference temperature that was previously used in the Strawberry Tree ™ system. The error inherent with the thermocouple wires is ±1°C.

3.4.2. Pressure Measurements

Four pressure transducers are installed on the refrigeration loop and test section. Three of the transducers are absolute pressure transducers and are located at the exit of the compressor vapor line, at the inlet to the pre-heater, and at the inlet of the test section. The other transducer is a differential transducer, which measures the pressure drop across the test section. The pre-heater inlet transducer is a BEC strain-gage type transducer (GP8-46DW-D-*-C-3) with a range of 0-300 psig (0-2100 kPa) and an accuracy of ±0.75% full scale. The test section inlet pressure transducer is an Omega thin film polysilicon strain gage of stainless steel construction (PX215-300AI). It has a range of 0-300 psia (0-2100 kPa) with an accuracy of ±0.25% full scale. Setra manufactures the compressor exit pressure transducer (280E) that has a range of 0-1000 psia (0-6900 kPa) with an accuracy of ±0.20% full scale. Lastly, the differential pressure transducer was manufactured by Sensotec (Z/1309-12-01), and has a range of 0-5 psid (0-35 kPa) with an accuracy of ±0.25% full scale. All of the transducers except the Setra have a 4-20 mA output. The Setra has a 0 to 5 Vdc output.

3.4.3. Mass Flow Measurements

The liquid mass flow meter used is a model D12 manufactured by Micromotion®. The meter measures the flow rate by the vibration frequency of a U-tube located inside. The meter delivers a specific current depending on the vibrational frequency of the U-tube. The data acquisition program, with the use of a 250 ohm resistor, reads the corresponding voltage, and a curve fit is used to determine the mass flow rate. The meter has a maximum flow range of 0 to 0.083 kg/s. An accuracy of ±0.2% of the rate is obtained from the flow meter.

A second flow meter is used in the compressor line. This is an Elite® vapor Micromotion® sensor (CMF025M314NU). The sensor measures the flow using the Coriolis effect. The meter's nominal flow range is from 0 to 0.94 kg/s. The maximum measurable flow rate is 1.89 kg/s. The accuracy within these ranges is ±0.50% of the vapor flow rate.

3.4.4. Power Measurements

Three power transducers manufactured by the Ohio Semitronics company are used on the experimental facility. The heat flux to the test section is measured by a PC5-49D292 power transducer. The heat input to the pre-heater is measured by two different transducers. One of the transducers (PC5-50D292) is used to measure the power delivered by the circuits that are switch controlled. The other (PC5-010D) is used to measure the power delivered by the variac controlled circuit. Each of these power transducers was tested at the factory to have an uncertainty of 0.2% full scale reading.

3.4.5. Calculated Parameters

Several quantities cannot be measured directly and these must be calculated within the data acquisition program. These include the test section heat flux, mass flux, the enthalpy entering the pre-heater, the enthalpy exiting the compressor, and the test section inlet quality.

3.4.5.1. Mass Flux and Heat Flux

The mass flux is determined by summing the mass flow rates recorded by the Micromotion® devices and then dividing by the test section cross sectional area. The test section heat flux is calculated in much the same way dividing the energy added to the test section by the heater strips by the surface area of the test section.

3.4.5.2. Pre-heater Inlet Enthalpy

The enthalpy at the inlet of the pre-heater was approximated by knowing the temperature and pressure at the pre-heater inlet and using the following relation:

$$h_{sub} = h_l + v_l * (P_{sub} - P_l) \qquad (3.1)$$

The internal energy is assumed to be the same for both the subcooled and saturated liquid states. A small correction is made for the Pv term in enthalpy, however. As seen, the $P_l v_l$ term is subtracted while the $P_{sub} v_l$ term is added. The $P_{sub} v_l$ term is very nearly exact since v_l approximately equals v_{sub} in subcooled conditions.

3.4.5.3. Vapor Line Exit Enthalpy

The vapor refrigerant coming from the compressor is in superheat. Thus, the enthalpy just prior to mixing is known by the temperature and pressure there. Since HP VEE does not have refrigerant table lookup capability, curve fits were used. In order to do this, various saturation pressures were calculated from a range of –10 to 50°C. The enthalpies of a superheated refrigerant were calculated at the saturated pressure and a temperature higher than saturation. The range of -10 to 50°C was chosen for one main reason. Although the test section saturation testing temperature is 5°C, the test section saturation temperature ranges from approximately 0 to 30°C during operation. Since these temperatures were used to calculate the saturated pressures which were then used in calculating the superheated vapor, a wider range from -10 to 50°C was chosen to include a factor of safety. In order for the vapor to enter the saturated mixture in superheated conditions, the vapor must be at a temperature higher than the saturation temperature for a saturated mixture pressure, however. Thus, temperatures from 5 to 55°C were chosen as the vapor temperature leaving the vapor line. This is reasonable since the observed temperatures entering the mixture typically range from 15 to 45°C.

The code used in developing these curves is given in Appendix D and the curves for R134a and R410A are seen in Figure D.1. and Figure D.2. The curves were fitted with quadratic trendlines obtaining equations with the following form:

$$h = A^* P^2 + B * P + C \tag{3.2}$$

where A, B, and C are coefficients with units of $m^5/(kN\ kg)$, m^3/kg, and kJ/kg, respectively. The pressure, P, has units of kPa.

In order to determine how temperature affects these curves, the coefficients of these trendlines were then plotted with temperature and trendlines obtained as seen in Figure D.3. and Figure D.4. Using these curves, the accuracy of the curve fits were found to be ±0.3%. The equations for the coefficients are seen in Table 3.1.

Table 3.1. Enthalpy Coefficients for R134a and R410A

R134A		R410A
Equation	Coefficient	Equation
$A = -8E\text{-}9*T^2 + 1E\text{-}6*T - 3E\text{-}5$	A [m^5/(kN kg)]	$A = 5E\text{-}10*T^2 + 2E\text{-}8*T - 5E\text{-}6$
$B = 3E\text{-}6*T^2 - 0.0002*T - 0.014$	B [m^3/kg]	$B = -3E\text{-}6*T^2 + 0.0004*T - 0.0226$
$C = 0.0003*T^2 + 0.8409*T + 253.7$	C [kJ/kg]	$C = 0.001*T^2 + 0.732*T + 298.73$
Note: Temperatures are in degrees Celsius.		

3.4.5.4. Test Section Inlet Quality

The inlet enthalpy to the test section is determined using Equation 3.3 as seen below:

$$\dot{m}_{in}\, h_{Test\_Section\_Inlet} = \dot{m}_{vapor\_line}\, h_{vapor\_line} + \dot{m}_{liquid\_line}\, h_{liquid\_line} + \dot{Q}_{Pre-heat} \qquad (3.3)$$

where

$$\dot{m}_{in} = \dot{m}_{vapor\_line} + \dot{m}_{liquid\_line} \qquad (3.4)$$

The enthalpy of the vapor line is that at the exit of the compressor as given in Section 3.4.5.3. and the enthalpy of the liquid line is that at the inlet to the pre-heater as given in Equation 3.1. The mass flow rates of the vapor and liquid lines are obtained from Micromotion® devices. The pre-heater power is measured by the power transducers.

To determine the test section inlet quality due to the pump and pre-heater alone, the vapor term due to the compressor is zero. The remaining equation used to calculate the enthalpy at the inlet of the test section is then:

$$h_{Test\_Section\_Inlet} = \frac{\dot{Q}_{Pre-heat}}{\dot{m}_{in}} + h_{sub} \tag{3.5}$$

where $\dot{m}_{in}$ equals $\dot{m}_{liquid\_line}$. In order to solve for the enthalpy at the inlet of the test section, the pre-heater inlet temperature and pressure must be known. The enthalpy at that subcooled pre-heater inlet point is then calculated by a curve fit of the saturated liquid enthalpy and Equation 3.1. Next, the enthalpy at the exit of the pre-heater is found by utilizing the power input by the pre-heater. The enthalpy of this fluid that flows adiabatically from the pre-heater exit through the insulated tubing to the test sections is assumed to be the enthalpy of the refrigerant entering the test section from the liquid line. This enthalpy is then used to calculate the test section inlet quality as seen in the following equation:

$$x = \frac{h_{Test\_Section\_Inlet} - h_l}{h_v - h_l} \tag{3.6}$$

The saturated liquid and saturated vapor enthalpies at the test section inlet temperature are calculated using curve fits.

A mixture calculation is necessary in order to calculate the test section inlet quality when the quality of the inlet flow is due to mixing of both liquid from the pump and vapor from the compressor lines. Using Equation 3.3 the test section inlet enthalpy can be calculated. The inlet enthalpy is then used with Equation 3.6 to determine the inlet quality.

Engineering Equation Solver (EES) v5.029, a f-chart software program developed by S.A. Klein and F.L. Alvarado [1992-1999], was used to develop the property curve fits for both R134a and R410A. The program uses the Martin-Hou equation of state to determine the property values for both R134a and R410A.

3.5. System Preparation, Start-up, and Operation

After the new evaporator loop was assembled, various steps were necessary to prepare and operate the experimental loop. This section discusses these steps as well as the ones for operation of the experimental apparatus.

3.5.1. System Preparation

Before the system could be operated, various steps had to be taken. The system was checked for leaks. Compressed nitrogen gas was first used to pressurize the system to 1000 kPa. The fittings and joints would then be checked for leaks using Big Blu®, a micro leak detector from Refrigeration Technologies. This fluid would indicate a leak by bubbling or foaming. If no leaks were found using Big Blu®, the system would be sectioned off with each section containing a pressure transducer as well as a thermocouple. The mass of the nitrogen would then be calculated within the system using the ideal gas equation. If this mass remained constant for more than two hours then the system was considered leak-free. Since the apparatus was sectioned off, if there was a leak, the leak could be localized to a particular section. At this point Big Blu® could be reused at each fitting and more carefully checked for foaming, or the nitrogen in the section could be released and R134a added to the system to a pressure of 300 kPa. The

Yokogawa universal service leak detector (H-10G) could then be used in locating the leaks in the system. This device would give a steady beep that would increase in frequency upon the detection of the refrigerant. Care must be taken if too much refrigerant is in the near vicinity of the detector, however. This may cause the device to falsely signal a leak.

Many of the leaks found involved solder joints. This was particularly the case with the larger solder joints, such as those on the separator tank. Some of the compression fittings also had to be tightened down to stop the leaks. Also, applying teflon tape to the threaded connections or replacing the ferrules helped in some cases. One surprising source of leakage was through the stem of the Hoke needle valve, however. The gland nut on the valve stem had not been tightened causing the refrigerant to leak. This fitting should be tightened down to a point where leaks are eliminated, but care should be taken to not crush the teflon seal that sits under the fitting.

After attempting to eliminate all of the leaks, nitrogen would be used to do a final check on the system. The system would be considered leak-free after the mass of nitrogen within the system would remain constant for two hours. At this point, the system could then be evacuated and the refrigerant added to the system through the valve by the separator tank. Ice should first be added to the bucket surrounding the separator tank before charging the system.

3.5.2. System Start-up and Operation

The following steps should be taken in order to start-up the apparatus and obtain the desired test conditions. First, ice should be added to the bucket enclosing the

separator tank. This will help condense the refrigerant and ensure enough refrigerant is available for the pump. Next, the data acquisition system should be turned on with the corresponding Microsoft Excel template. This will allow monitoring of the loop conditions. After allowing the tank to cool for at least 5 minutes, all the valves for the liquid lines should be opened and then the pump may be turned on and set to the second level on the control box. The mass flow rate of the liquid should be monitored to check for cavitation. If there is no flow, the pump should be turned off and the separator tank should be given additional time for cooling. The vapor bypass and damping tank valves may also be open if the vapor line contains any liquid. After the pump is operational, the compressor head should be heated with a heat gun. This is done to vaporize any liquid that may be entrained in the compressor. After this, all the valves on the damping tanks should be opened. Then the compressor should be turned on and the valve furthest downstream in the vapor line at the mixing point should be opened. The chiller pump and compressor should be turned on as well as the water lines opened to cool down the refrigerant and remove any additional heat added by the operation of the system. Opening the valve for the water by two to three revolutions should provide enough cold water for cooling.

In order to obtain a certain test section inlet mass flux and quality with an inlet temperature of 5°C, an EES code was written to approximate the liquid and vapor flow rates necessary to get to certain specified mass flux and quality conditions. This code is given in Appendix E. The pump driver control as well as the liquid bypass valve can be adjusted to reach the desired liquid flow rate. The vapor flow rate can be controlled by adjusting the vapor bypass valve or slightly adjusting the vapor valve at the mixing point.

Both closing the vapor bypass valve and opening the valve at the mixing point will increase the vapor flow rate.

In order to get the test section inlet temperature to 5°C, two heat exchangers are used. One heat exchanger is located downstream of the test section. This heat exchanger removes the heat added from the pre-heater, test section heaters, and the compressor. This heat exchanger requires the most cooling so the valve for the propylene glycol is kept completely open. The other heat exchanger is downstream of the compressor. This heat exchanger is necessary to keep the vapor temperature at a reasonable temperature while mixing. Very little glycol flow is needed here. The glycol flow valve for this heat exchanger should be opened only a very small amount. If the test section inlet temperature drops below 5°C, this valve can then be shut to raise the temperature back to 5°C.

3.6. Figures

The test apparatus schematic for the new loop is included here. A schematic of the new chiller system used in this loop is included as well.

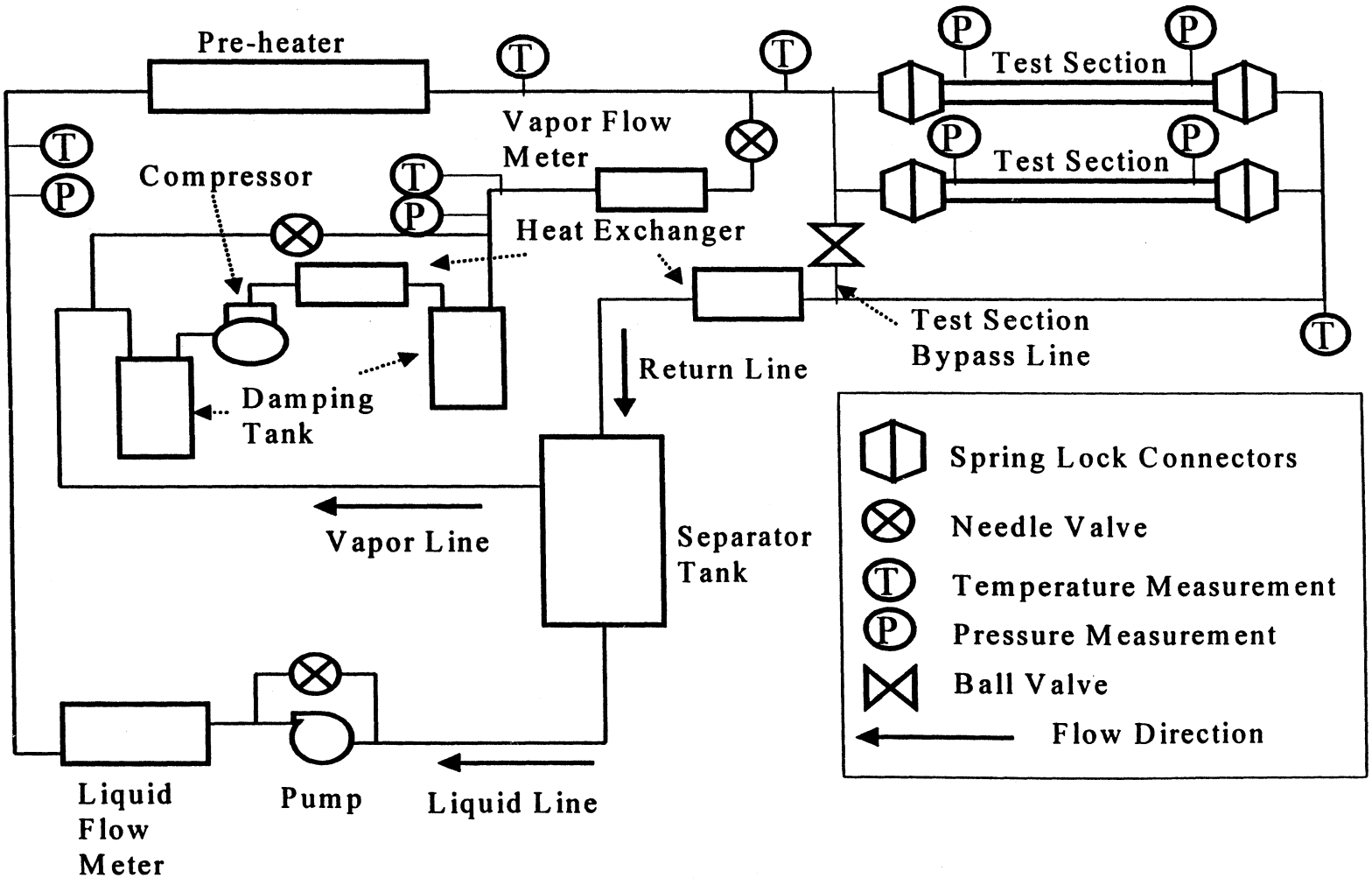

Figure 3.1. New Loop Schematic

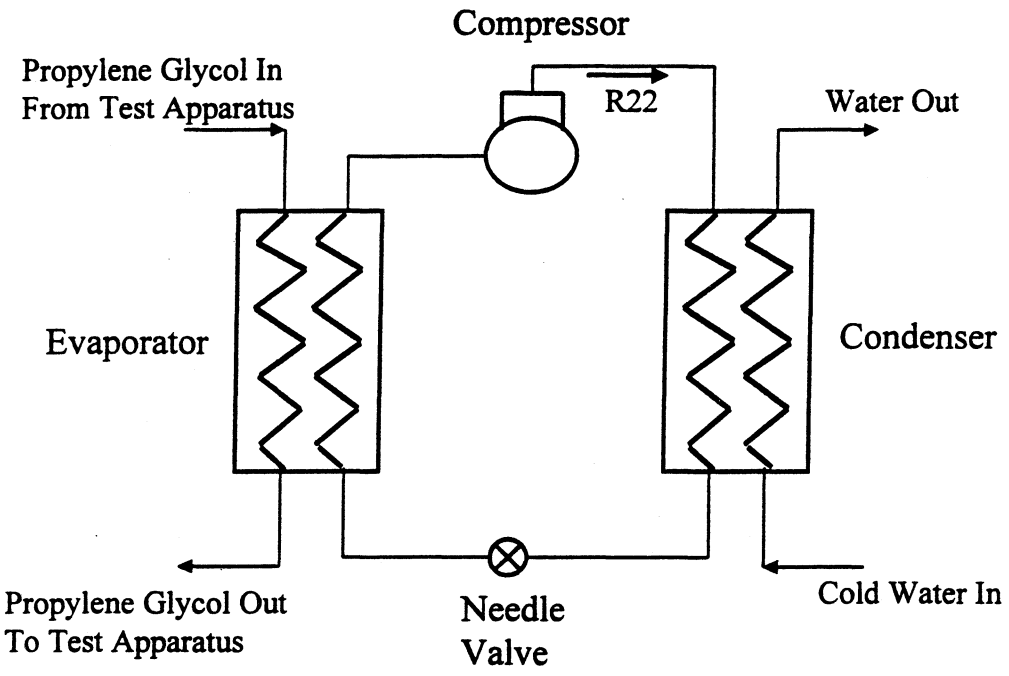

Figure 3.2: New Chiller System

3.7. Bibliography

Wattelet, J. P., J. P. Renie, and J. C. Chato. 1990. Design, Building, and Baseline Testing of an Apparatus Used to Measure Evaporation Characteristics of Ozone-Safe Refrigerants. ACRC TR-2, Air Conditioning and Refrigeration Center, University of Illinois, Urbana.

Wilson, M. J., T. A. Newell, and J. C. Chato. 1998. Experimental Investigation of Void Fraction During Horizontal Flow in Larger Diameter Refrigeration Applications. ACRC TR-140, Air Conditioning and Refrigeration Center, University of Illinois, Urbana.

Yashar, D. A., T. A. Newell, and J. C. Chato. 1998. Experimental Investigation of Void Fraction During Horizontal Flow in Smaller Diameter Refrigerant Applications. ACRC TR-141, Air Conditioning and Refrigeration Center, University of Illinois, Urbana.

Chapter 4

Conclusion

The initial study on return bends has been completed and the construction of the new apparatus has also been completed. The findings and recommendations follow.

Various return bend effects were observed in the study. Refrigerants R134a and R410A were tested over a range of qualities from 5 to 70% and a range of mass fluxes from 65 to 440 kg/m^2 s under an evaporative inlet temperature of 5°C. Few effects on the return bends were detected from the void fraction study. Most of the trends observed were from the pressure drop analysis. The pressure drop was observed to increase with both quality and mass flux. Although much less prominent, orientation of the bends also showed some effects on pressure drop. The pressure drop tended to increase from downflow to upflow conditions. Pressure drops from this study were considerably more than that from previous studies. This is most likely due to the construction of the test section as well as the size of the return bend in this study.

A complementary study in condenser conditions may show significant effects in both void fraction and pressure drop. With a greater amount of liquid in the return bends, the vapor shearing effects as well as the greater changes in momentum may cause greater effects.

The new experimental apparatus for evaporative two-phase conditions was constructed and operated at the University of Illinois at Urbana-Champaign. Although baseline results have not been completed, testing is in progress. Future work involves continued testing with pure refrigerants and different refrigerant-oil mixtures in straight

tubes and flat plate evaporators to continue previous work by De Guzman [1997] and Gupta [2000].

4.1. References

De Guzman, N. M., and J. C. Chato. 1997. Evaporative Heat Transfer Characteristics in a Vertical Channel with Obstructions. Air Conditioning and Refrigeration Center, University of Illinois, Urbana.

Gupta, S., T: A. Newell, and J. C. Chato. 2000. MS Thesis, Air Conditioning and Refrigeration Center, University of Illinois, Urbana.

Appendix A

EES Code for Calculation of Void Fraction

{Input the volume of the test section (Vts), diameter of the tube (D), and the number of void fraction calculations (n). The other inputs for the void fraction (alpha) measurements are input in a lookup table in EES. The empty mass (me), final mass (mf), pressure in the receiver tank at test section discharge (P), temperature of the test section at discharge (Tcel), mass flux (G), and quality (x) are input into the lookup table.}

```
t1=5 {deg C}
P1=Pressure(R134A,T=T1,x=0)

Vts=8.85*10^(-5) {m^3}
D=.006985 {m}

vg=VOLUME(R134A,T=T1,x=1) {m^3/kg}
vl=VOLUME(R134A,T=T1,x=0) {m^3/kg}
mul=viscosity(R134A,T=T1,P=P1+10)
mug=viscosity(R134A,T=T1,P=P1-10)

n=1
Duplicate i=1,n

me[i]=lookup(i,1)/1000 {kg}
mf[i]=lookup(i,2)/1000 {kg}
P[i]=lookup(i,3)+14.7 {in psi}
Pk[i]=P[i]*101.325/14.7 {kPa}
Tcel[i]=lookup(i,4) {deg C}

pho1[i]=density(R134A,T=Tcel[i],P=Pk[i]) {kg/m^3}
mm[i]=pho1[i]*Vts {kg...remaining mass}

mt[i]=mf[i]-me[i]+mm[i] {kg}

specVts[i]=Vts/mt[i] {m^3/kg}
xs[i]=quality(R134A,T=t1,v=specVts[i])

xs[i]=(((1-alpha[i])/alpha[i])*(vg/vl)+1)^(-1)

G[i]=lookup(i,5)
x[i]=lookup(i,6)/100
Xtt[i]=((1-x[i])/x[i])^.9*(vl/vg)^.5*(mul/mug)^.1
Fr[i]=((x[i]^3*G[i]^2*vg^2)/(9.81*D*(1-x[i])))^.5
End
```

Appendix B

Return Bend Void Fraction and Pressure Drop Data and Plots

This appendix presents the raw data as well as additional plots from the return bend testing. This testing was for both the R134a and R410A refrigerants as well as three orientations.

B.1. Tables

These are the tables containing the raw pressure drop and void fraction data for both refrigerants R134a and R410A. The mass flux, G, is for the 7.47 mm diameter tubes in the return bend test section. The inlet quality, x, is assumed to be the quality of the entire test section since testing was performed under adiabatic conditions. The Xtt is the Lockhart-Martinelli parameter. It is defined as:

$$X_{tt} = \left(\frac{1-x}{x}\right)^{0.9}\left(\frac{\rho_v}{\rho_l}\right)^{0.5}\left(\frac{\mu_l}{\mu_v}\right)^{0.1} \tag{B.1}$$

The Froude rate, Ft, is defined as:

$$Ft = \left[\frac{x^3 G^2}{\rho_v^2 gD(1-x)}\right]^{\frac{1}{2}} \tag{B.2}$$

The void fraction is found using:

$$\alpha = \frac{1}{1+\left(\frac{1-x_s}{x_s}\right)\left(\frac{\rho_v}{\rho_l}\right)} \tag{B.3}$$

where x_s is the static quality. The void fraction is calculated using the EES code found in Appendix A.

Table B.1. Void Fraction Data for R134a

Test Run	Refrigerant	Orientation	G (tube)	Inlet x	Xtt	Ft	Void Fraction
1	R134a	Up	66	0.1	1.171	0.5568	0.8494
2	R134a	Up	66	0.1	1.171	0.5568	0.8442
3	R134a	Up	66	0.5	0.1621	8.352	0.9531
4	R134a	Up	66	0.5	0.1621	8.352	0.9515
5	R134a	Up	131	0.1	1.171	1.114	0.8542
6	R134a	Up	131	0.1	1.171	1.114	0.845
7	R134a	Up	262	0.1	1.171	2.227	0.8423
8	R134a	Up	262	0.1	1.171	2.227	0.8617
9	R134a	Up	262	0.2	0.5644	6.681	0.886
10	R134a	Up	262	0.2	0.5644	6.681	0.8919
11	R134a	Up	262	0.3	0.3474	13.12	0.9219
12	R134a	Up	262	0.3	0.3474	13.12	0.9202
13	R134a	Up	437	0.05	2.294	1.277	0.8024
14	R134a	Up	437	0.05	2.294	1.277	0.8135
15	R134a	Up	437	0.1	1.171	3.712	0.8682
16	R134a	Up	437	0.1	1.171	3.712	0.8727
17	R134a	Horizontal	66	0.1	1.171	0.5568	0.7868
18	R134a	Horizontal	66	0.1	1.171	0.5568	0.8079
19	R134a	Horizontal	131	0.1	1.171	1.114	0.8342
20	R134a	Horizontal	131	0.1	1.171	1.114	0.8549
21	R134a	Horizontal	131	0.7	0.0756	35.72	0.9771
22	R134a	Horizontal	131	0.7	0.0756	35.72	0.9706
23	R134a	Horizontal	262	0.1	1.171	2.227	0.7979
24	R134a	Horizontal	262	0.1	1.171	2.227	0.845
25	R134a	Horizontal	262	0.1	1.171	2.227	0.8455
26	R134a	Horizontal	262	0.2	0.5644	6.681	0.8801
27	R134a	Horizontal	262	0.2	0.5644	6.681	0.8733
28	R134a	Horizontal	262	0.3	0.3474	13.12	0.9021
29	R134a	Horizontal	262	0.3	0.3474	13.12	0.9211
30	R134a	Horizontal	437	0.05	2.294	1.277	0.7453
31	R134a	Horizontal	437	0.05	2.294	1.277	0.8091
32	R134a	Horizontal	437	0.05	2.294	1.277	0.7929
33	R134a	Horizontal	437	0.1	1.171	3.712	0.8344
34	R134a	Horizontal	437	0.1	1.171	3.712	0.8373
35	R134a	Down	66	0.1	1.171	0.5568	0.8032
36	R134a	Down	66	0.1	1.171	0.5568	0.8465
37	R134a	Down	66	0.1	1.171	0.5568	0.835
38	R134a	Down	66	0.3	0.3474	3.28	0.9089
39	R134a	Down	66	0.3	0.3474	3.28	0.9334
40	R134a	Down	131	0.1	1.171	1.114	0.8346
41	R134a	Down	131	0.1	1.171	1.114	0.8362
42	R134a	Down	131	0.1	1.171	1.114	0.8334
43	R134a	Down	262	0.1	1.171	2.227	0.8375
44	R134a	Down	262	0.1	1.171	2.227	0.8313
45	R134a	Down	262	0.2	0.5644	6.681	0.8996

Table B.1. (Continued)

46	R134a	Down	262	0.2	0.5644	6.681	0.8851
47	R134a	Down	437	0.05	2.294	1.277	0.7598
48	R134a	Down	437	0.05	2.294	1.277	0.7505
49	R134a	Down	437	0.1	1.171	3.712	0.8165
50	R134a	Down	437	0.1	1.171	3.712	0.8372
51	R134a	Down	437	0.1	1.171	3.712	0.8711
52	R134a	Down	437	0.1	1.171	3.712	0.8775
53	R134a	Down	437	0.1	1.171	3.712	0.8508.

Table B.2. Void Fraction Data for R410A

Test Run	Refrigerant	Orientation	G (tube)	Inlet x	Xtt	Ft	Void Fraction
1	R410A	Up	66	0.1	1.632	0.2324	0.673
2	R410A	Up	66	0.1	1.632	0.2324	0.6769
3	R410A	Up	66	0.5	0.2259	3.487	0.8908
4	R410A	Up	66	0.5	0.2259	3.487	0.9036
5	R410A	Up	131	0.1	1.632	0.4649	0.667
6	R410A	Up	131	0.1	1.632	0.4649	0.6933
7	R410A	Up	262	0.1	1.632	0.9297	0.6956
8	R410A	Up	262	0.1	1.632	0.9297	0.7047
9	R410A	Up	262	0.2	0.7866	2.789	0.785
10	R410A	Up	262	0.2	0.7866	2.789	0.7808
11	R410A	Up	262	0.3	0.4843	5.478	0.8556
12	R410A	Up	262	0.3	0.4843	5.478	0.8334
13	R410A	Up	262	0.5	0.2259	13.95	0.9112
14	R410A	Up	262	0.5	0.2259	13.95	0.9079
15	R410A	Up	437	0.05	3.197	0.5332	0.6215
16	R410A	Up	437	0.05	3.197	0.5332	0.5928
17	R410A	Up	437	0.05	3.197	0.5332	0.6222
18	R410A	Up	437	0.1	1.632	1.55	0.6903
19	R410A	Up	437	0.1	1.632	1.55	0.7273
20	R410A	Up	437	0.1	1.632	1.55	0.7037
21	R410A	Horizontal	66	0.1	1.632	0.2324	0.6479
22	R410A	Horizontal	66	0.1	1.632	0.2324	0.6607
23	R410A	Horizontal	66	0.5	0.2259	3.486	0.8968
24	R410A	Horizontal	66	0.5	0.2259	3.486	0.9235
25	R410A	Horizontal	131	0.1	1.632	0.4648	0.6835
26	R410A	Horizontal	131	0.1	1.632	0.4648	0.6567
27	R410A	Horizontal	262	0.1	1.632	0.9299	0.6725
28	R410A	Horizontal	262	0.1	1.632	0.9299	0.6566
29	R410A	Horizontal	262	0.2	0.7866	2.79	0.78
30	R410A	Horizontal	262	0.2	0.7866	2.79	0.7626
31	R410A	Horizontal	262	0.3	0.4843	5.479	0.8513

Table B.2. (Continued)

32	R410A	Horizontal	262	0.5	0.2259	13.95	0.9195
33	R410A	Horizontal	262	0.5	0.2259	13.95	0.9164
34	R410A	Horizontal	437	0.05	3.197	0.5332	0.6154
35	R410A	Horizontal	437	0.05	3.197	0.5332	0.5717
36	R410A	Horizontal	437	0.05	3.197	0.5332	0.6054
37	R410A	Horizontal	437	0.1	1.632	1.549	0.7007
38	R410A	Horizontal	437	0.1	1.632	1.549	0.6983
39	R410A	Down		0.1	1.632	0.2324	0.7233
40	R410A	Down	66	0.1	1.632	0.2324	0.7201
41	R410A	Down	66	0.5	0.2259	3.486	0.8945
42	R410A	Down	66	0.5	0.2259	3.486	0.9176
43	R410A	Down	66	0.1	1.632	0.4648	0.7168
44	R410A	Down	131	0.1	1.632	0.4648	0.688
45	R410A	Down	131	0.1	1.632	0.9299	0.6596
46	R410A	Down	262	0.1	1.632	0.9299	0.7222
47	R410A	Down	262	0.2	0.7866	2.79	0.7852
48	R410A	Down	262	0.2	0.7866	2.79	0.8319
49	R410A	Down	262	0.2	0.7866	2.79	0.7753
50	R410A	Down	262	0.3	0.4843	5.479	0.8397
51	R410A	Down	262	0.3	0.4843	5.479	0.8471
52	R410A	Down	262	0.5	0.2259	13.95	0.9112
53	R410A	Down	262	0.5	0.2259	13.95	0.909
54	R410A	Down	262	0.05	3.197	0.5332	0.6307
55	R410A	Down	437	0.05	3.197	0.5332	0.597
56	R410A	Down	437	0.1	1.632	1.549	0.6825
57	R410A	Down	437	0.1	1.632	1.549	0.6752

Table B.3. Pressure Drop Data for R134a

Test Run	Refrigerant	Orientation	G (tube)	Inlet x	Pressure Drop (kPa) (Test Section)	Pressure Drop (kPa) (Return Bend)
1	R134a	Up	66	0.25	0.944	0.279782
2	R134a	Up	66	0.3	1.082	0.313079
3	R134a	Up	66	0.3	0.983	0.280079
4	R134a	Up	66	0.3	1.094	0.317079
5	R134a	Up	131	0.1	1.853	0.596354
6	R134a	Up	131	0.3	3.663	1.084245
7	R134a	Up	131	0.3	3.687	1.092245
8	R134a	Up	131	0.5	7.527	2.333275
9	R134a	Up	131	0.7	9.703	2.876344
10	R134a	Up	262	0.1	5.067	1.688053
11	R134a	Up	437	0.05	9.318	3.104108
12	R134a	Up	437	0.05	7.827	2.607108

Table B.3. (Continued)

13	R134a	Up	437	0.05	8.148	2.714108
14	R134a	Up	437	0.1	15.742	5.243849
15	R134a	Up	437	0.1	14.128	4.705849
16	R134a	Up	437	0.1	14.408	4.799182
17	R134a	Horizontal	66	0.1	0.367	0.122333
18	R134a	Horizontal	66	0.1	0.478	0.159333
19	R134a	Horizontal	131	0.1	1.232	0.410143
20	R134a	Horizontal	131	0.2	2.251	0.749387
21	R134a	Horizontal	131	0.3	3.503	1.164619
22	R134a	Horizontal	131	0.3	3.611	1.200619
23	R134a	Horizontal	131	0.5	7.399	2.462355
24	R134a	Horizontal	131	0.5	7.811	2.599689
25	R134a	Horizontal	131	0.5	7.802	2.596689
26	R134a	Horizontal	131	0.5	8.366	2.784689
27	R134a	Horizontal	131	0.7	9.215	3.062976
28	R134a	Horizontal	131	0.7	9.543	3.172309
29	R134a	Horizontal	262	0.1	5.617	1.870441
30	R134a	Horizontal	262	0.1	5.04	1.678108
31	R134a	Horizontal	262	0.1	4.326	1.440108
32	R134a	Horizontal	262	0.2	9.556	3.181849
33	R134a	Horizontal	262	0.2	9.38	3.123182
34	R134a	Horizontal	262	0.2	11.439	3.809516
35	R134a	Horizontal	262	0.2	9.78	3.256516
36	R134a	Horizontal	262	0.3	15.342	5.102687
37	R134a	Horizontal	437	0.05	8.618	2.872667
38	R134a	Horizontal	437	0.1	15.641	5.206169
39	R134a	Horizontal	437	0.1	17.193	5.723502
40	R134a	Horizontal	437	0.1	16.514	5.497169
41	R134a	Down	66	0.1	0.214	0.051043
42	R134a	Down	66	0.1	0.276	0.071709
43	R134a	Down	66	0.1	0.24	0.059709
44	R134a	Down	66	0.3	0.985	0.241372
45	R134a	Down	66	0.3	0.807	0.182038
46	R134a	Down	131	0.1	1.141	0.303161
47	R134a	Down	131	0.1	0.736	0.168161
48	R134a	Down	131	0.3	4.323	1.107516
49	R134a	Down	131	0.3	4.035	1.011516
50	R134a	Down	131	0.5	7.348	1.721708
51	R134a	Down	131	0.5	6.071	1.296041
52	R134a	Down	262	0.1	4.701	1.220694
53	R134a	Down	262	0.1	4.68	1.213694
54	R134a	Down	262	0.2	10.324	2.605677
55	R134a	Down	437	0.05	8.206	2.275277
56	R134a	Down	437	0.1	13.209	3.486694
57	R134a	Down	437	0.1	14.638	3.963027
58	R134a	Down	437	0.1	19.737	5.662694

Table B.3. (Continued)

59	R134a	Down	437	0.1	16.005	4.418694
60	R134a	Down	437	0.1	15.165	4.138694

Table B.4. Pressure Drop Data for R410A

Test Run	Refrigerant	Orientation	G (tube)	Inlet x	Pressure Drop (Test Section)	Pressure Drop (Return Bend)
1	R410A	Up	66	0.1	0.837	0.265544
2	R410A	Up	66	0.1	0.876	0.278544
3	R410A	Up	131	0.1	1.274	0.373372
4	R410A	Up	131	0.1	0.979	0.275038
5	R410A	Up	131	0.3	2.191	0.540612
6	R410A	Up	131	0.5	3.441	0.743916
7	R410A	Up	131	0.7	4.617	0.859187
8	R410A	Up	262	0.1	2.88	0.728666
9	R410A	Up	262	0.1	2.951	0.752333
10	R410A	Up	262	0.2	4.752	1.075028
11	R410A	Up	262	0.2	4.793	1.088694
12	R410A	Up	262	0.3	7.019	1.474105
13	R410A	Up	262	0.3	7.915	1.772772
14	R410A	Up	262	0.3	7.242	1.548438
15	R410A	Up	262	0.5	13.259	2.675095
16	R410A	Horizontal	66	0.1	0.072	0.010544
17	R410A	Horizontal	66	0.5	0.542	0.076655
18	R410A	Horizontal	66	0.5	0.539	0.075655
19	R410A	Horizontal	131	0.1	0.607	0.151038
20	R410A	Horizontal	131	0.1	0.492	0.112705
21	R410A	Horizontal	131	0.3	1.564	0.331612
22	R410A	Horizontal	131	0.5	3.055	0.615249
23	R410A	Horizontal	131	0.7	4.432	0.79752
24	R410A	Horizontal	262	0.1	2.727	0.677666
25	R410A	Horizontal	262	0.5	13.123	2.629762
26	R410A	Horizontal	262	0.5	12.739	2.501762
27	R410A	Horizontal	262	0.5	13.189	2.651762
28	R410A	Horizontal	262	0.5	12.976	2.580762
29	R410A	Horizontal	262	0.5	12.761	2.509095
30	R410A	Horizontal	437	0.1	8.455	2.237279
31	R410A	Horizontal	437	0.1	7.398	1.884945
32	R410A	Down	66	0.05	0.117	0.0302
33	R410A	Down	66	0.1	0.13	0.029877
34	R410A	Down	66	0.5	0.607	0.098321
35	R410A	Down	66	0.5	0.692	0.126655
36	R410A	Down	131	0.1	0.181	0.009038
37	R410A	Down	131	0.1	0.486	0.110705
38	R410A	Down	131	0.3	1.844	0.424946

Table B.4. (Continued)

39	R410A	Down	131	0.5	2.686	0.492249
40	R410A	Down	131	0.5	2.928	0.572916
41	R410A	Down	131	0.7	4.085	0.681853
42	R410A	Down	131	0.7	3.814	0.59152
43	R410A	Down	262	0.1	2.499	0.601666
44	R410A	Down	262	0.2	4.436	0.969694
45	R410A	Down	262	0.3	7.221	1.541438
46	R410A	Down	262	0.5	13.819	2.861762
47	R410A	Down	437	0.05	4.536	1.176991
48	R410A	Down	437	0.1	6.073	1.443279

B.2. Additional Plots

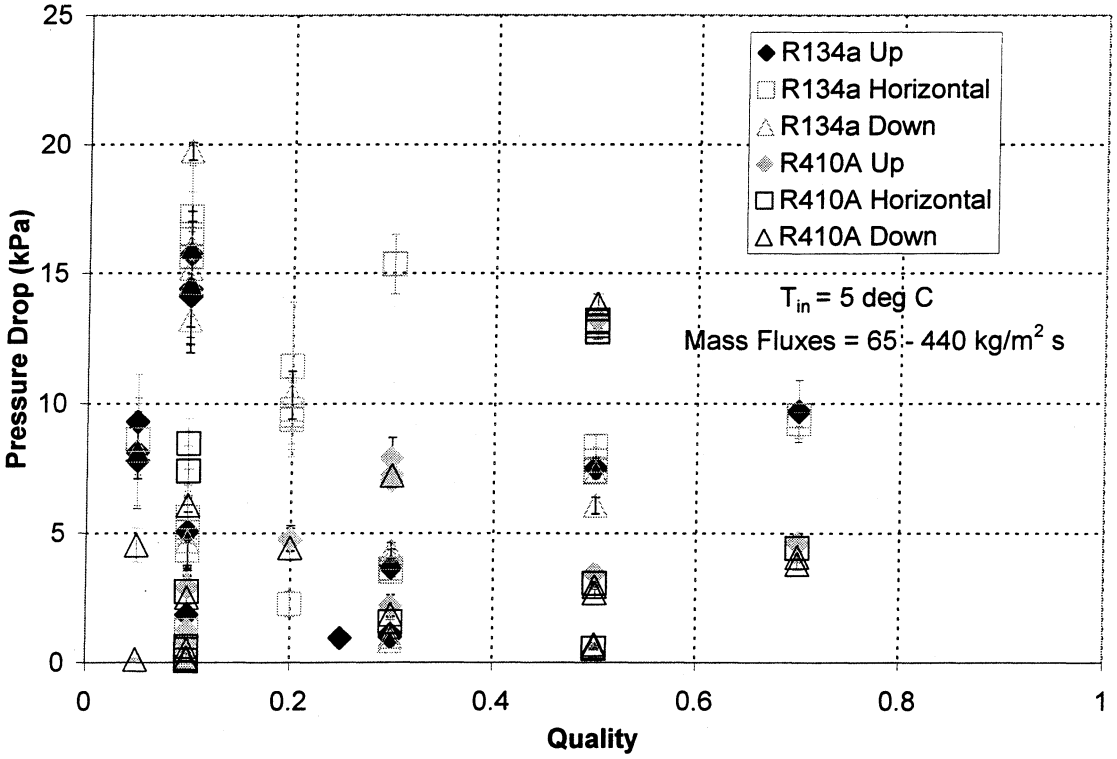

Figure B.1. Test Section Pressure Drop vs. Quality (All Mass Fluxes)

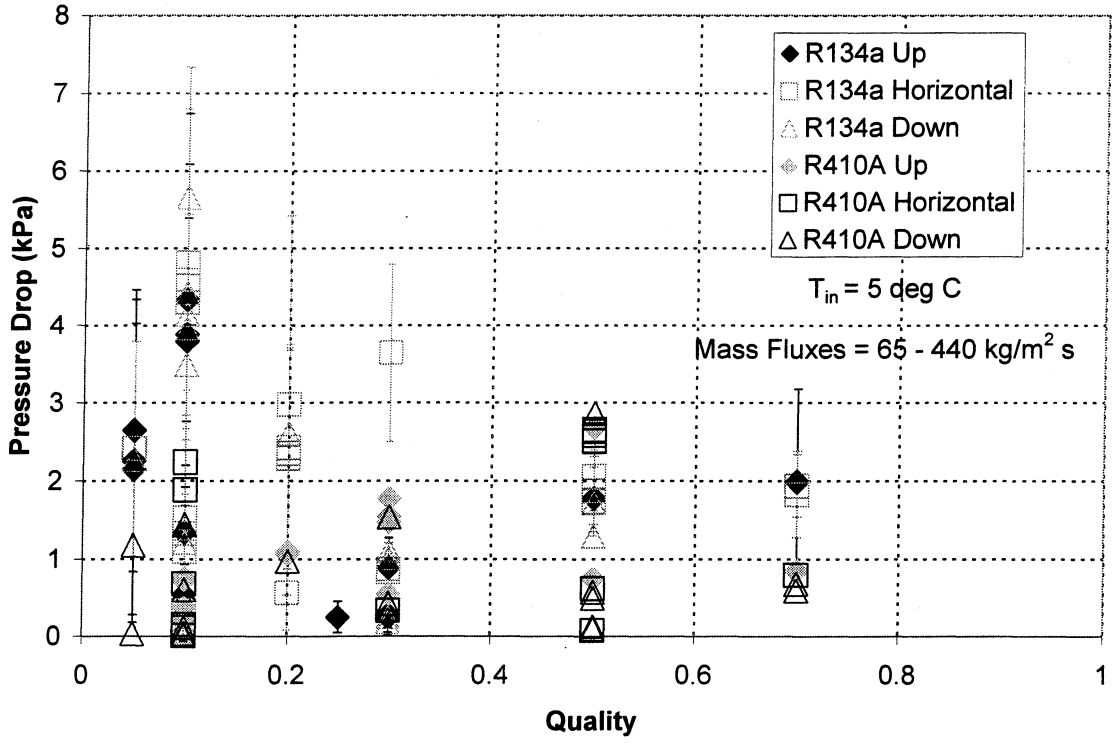

Figure B.2. Return Bend Pressure Drop vs. Quality (All Mass Fluxes)

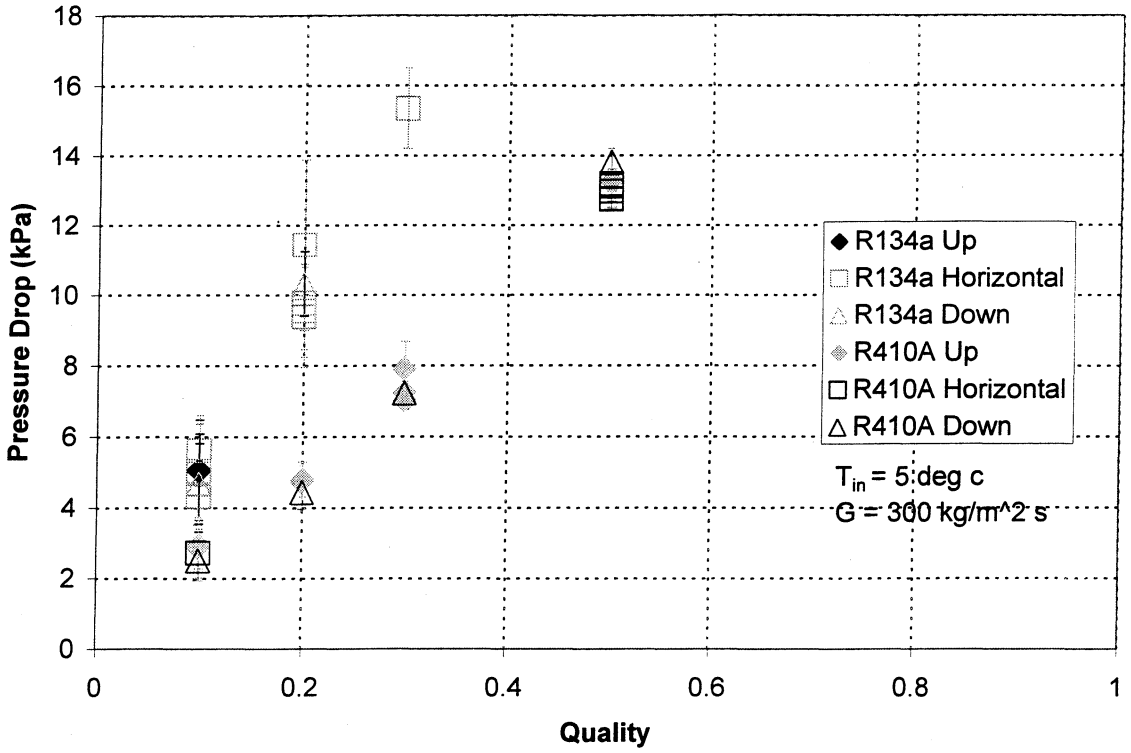

Figure B.3. Test Section Pressure Drop vs. Quality (G = 300 kg/m^2 s)

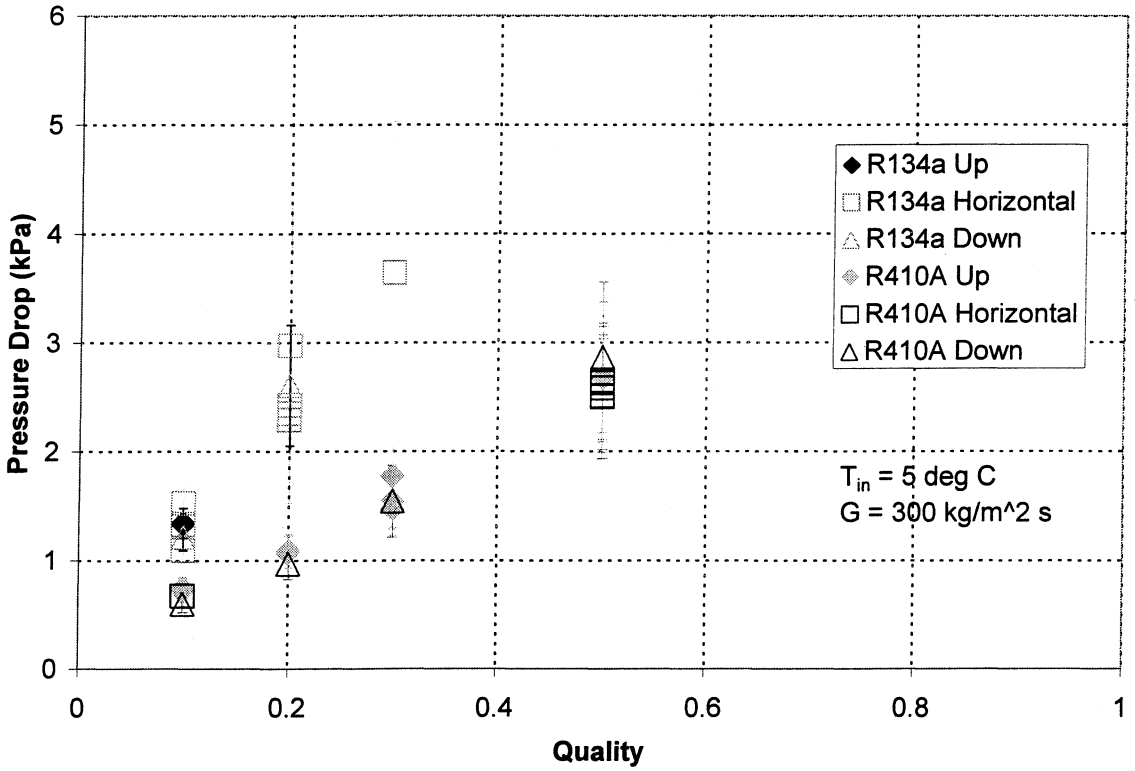

Figure B.4. Return Bend Pressure Drop vs. Quality (G = 300 kg/m^2 s)

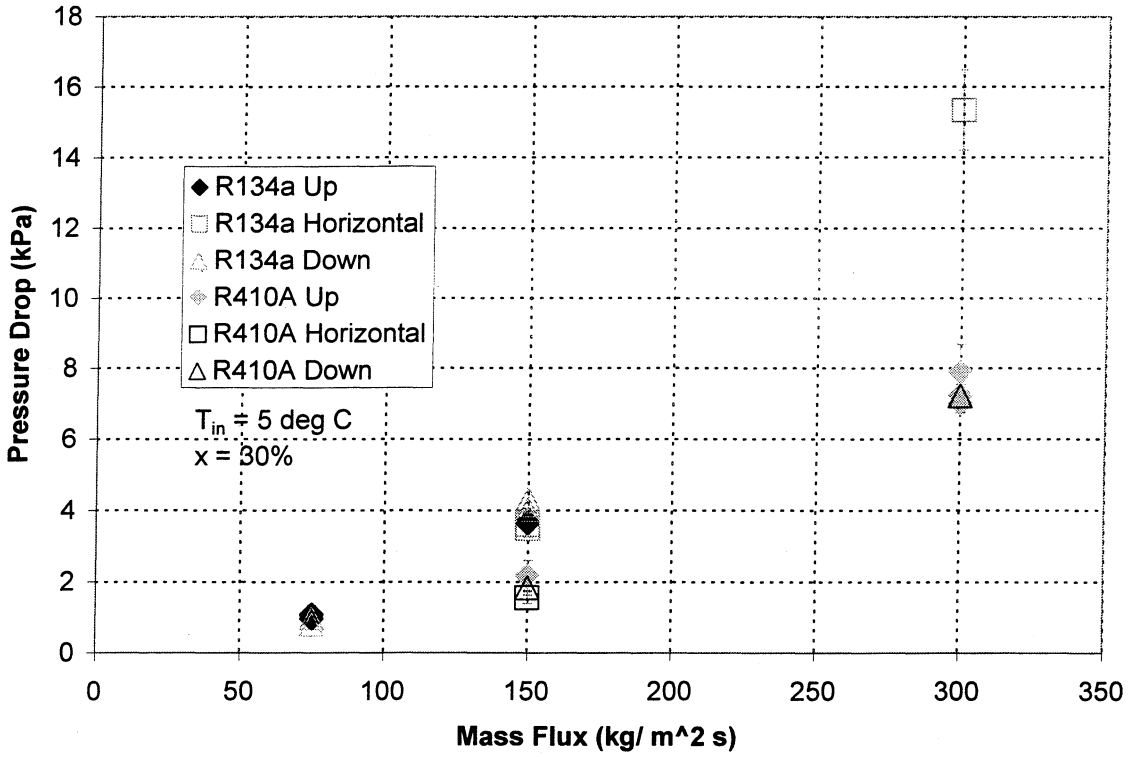

Figure B.5. Test Section Pressure Drop vs. Mass Flux (x = 30%)

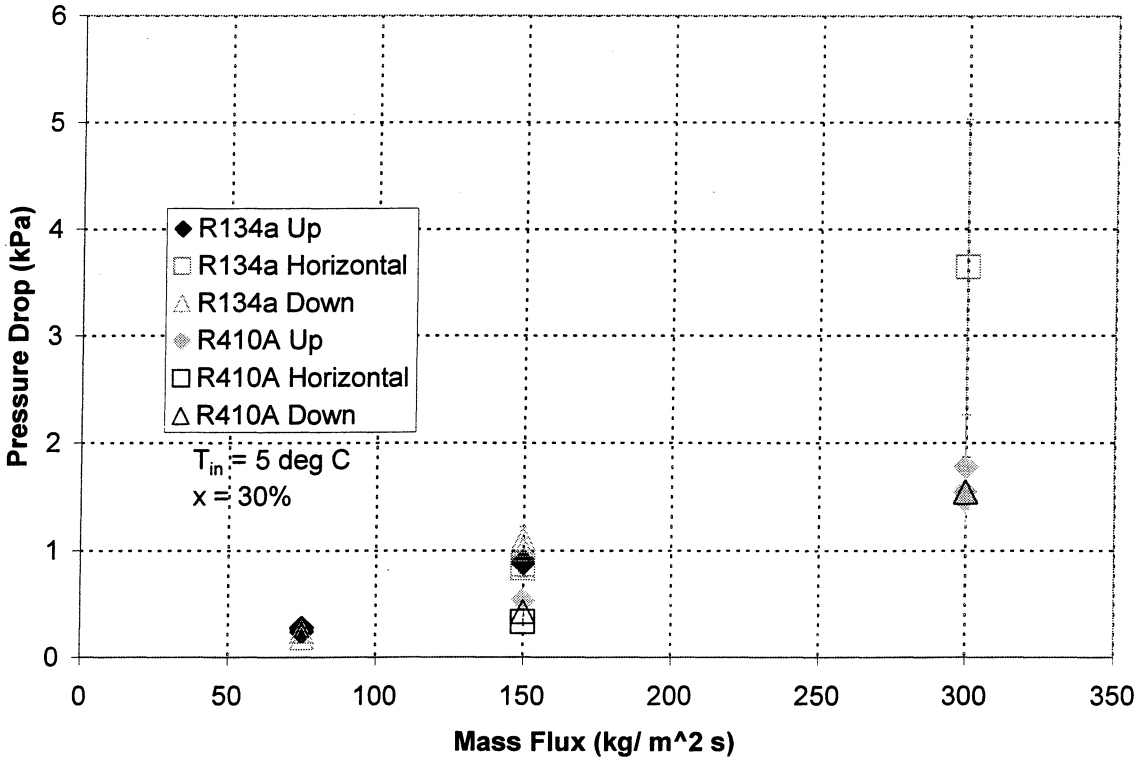

Figure B.6. Return Bend Pressure Drop vs. Mass Flux (x = 30%)

Appendix C

HP VEE Highlights

A sample subroutine in HP VEE used to measure temperature readings and output the results to Excel is shown in Figure C.1. Five types of command modules are present. The "Misc Temps – hp1326 (@70903)" box is a Direct I/O command box. This box commands the multimeter to measure specific variables from particular cards and terminals. Upon double clicking on this box, the box shown in Figure C.2. appears.

The first transaction line will take temperature measurements of T-type thermocouples at the addresses 300 to 305. The address 300 refers to the third multiplexer and terminal 00. The second transaction line reads these measurements and puts it into an array of 6 elements. By double clicking on these lines, these transaction lines are completed by filling in the blanks in a pop-up window. Although knowledge of some commands are necessary for these transactions, the use of the window modules keep the transactions simple. The commands can be found in the HP E1326B/E1411B Multimeter Command Reference found in the HP E1326B/E1411B 5.5-Digit Multimeter Module User's Manual.

The "Misc Temps" command box on the far right of Figure C.1. outputs the temperature measurements taken using the "Misc Temps – hp1326 (@70903)" box and the labels from "Misc Temp Labels" and "Misc Temp Label Input" boxes to Excel. This box is a User Object box. Upon double clicking on it, the box shown in Figure C.3. appears. Two Formula boxes and one To/From DDE box appears. The Formula boxes are used to manipulate the columns and rows where the data measurements will be output

in Excel. The To/From DDE box is the main interface between HP VEE and Excel. Under *application* in the DDE box, the software Excel is specified directing where HP VEE should output the data. The *topic* in the DDE box is the specific sheet name in Excel where the data will be output. Within the transaction lines are a couple of "write" commands that direct where the data will be written in Excel. The Formula boxes specified earlier define this location.

The other command boxes in Figure C.1. include a For Range box, a Text box, and several Formula boxes. The For Range command cycles through a particular range of numbers at the specified step increment. This was used to step through an entire array like the output from the temperature Direct I/O box. The Text box is used to input column headings for the Excel sheet. The Formula boxes are used to manipulate the variables. These boxes were used to separate the array of data and ensure the data is being entered in the correct location within Excel.

It may be necessary to add or remove certain thermocouples or sensors from the experimental loop. This should be performed in conjunction with changes in HP VEE and the connections to the jack panel. The temperature readings are taken in the second and third multiplexers. The terminals on the multiplexers are consecutively connected to the jack panels numbered 3 to 18 for the second multiplexer and 21 to 36 for the third multiplexer. The terminals are wired in such a way that the first panel number corresponds to the first terminal on the corresponding multiplexer. For example the thermocouple connected to jack panel #3 corresponds to multiplexer #2, terminal 00 while that connected to jack panel #4 would be at terminal 01. A thermocouple connected to jack panel #21 corresponds to multiplexer #3, terminal 00. From this, the

address of each thermocouple connected would be known. From Figure C.2. the addresses of 300 to 305 were recorded. This corresponds to the thermocouples connected to jack panels 21 to 26. Similarly if more thermocouples were needed, the thermocouples could be added and the address within the Direct I/O box changed in the transaction line.

Another change associated with this is the label output to Excel. This can be changed by typing over the labels in the text box. The boxes can also be double clicked and the number of labels changed.

Finally, a change must be made directing HP VEE to actually output the measurement to an Excel sheet. This change is made in a User Object box like that seen in Figure C.3. New command lines must be made in the To/From DDE box and additional formula boxes must be included to direct where each measurement should be output into Excel. A separate set of Formula boxes is required for each set of transactions in the Direct I/O command box.

C.1. Figures

The following figures include a sample HP VEE subroutine as well as command module boxes.

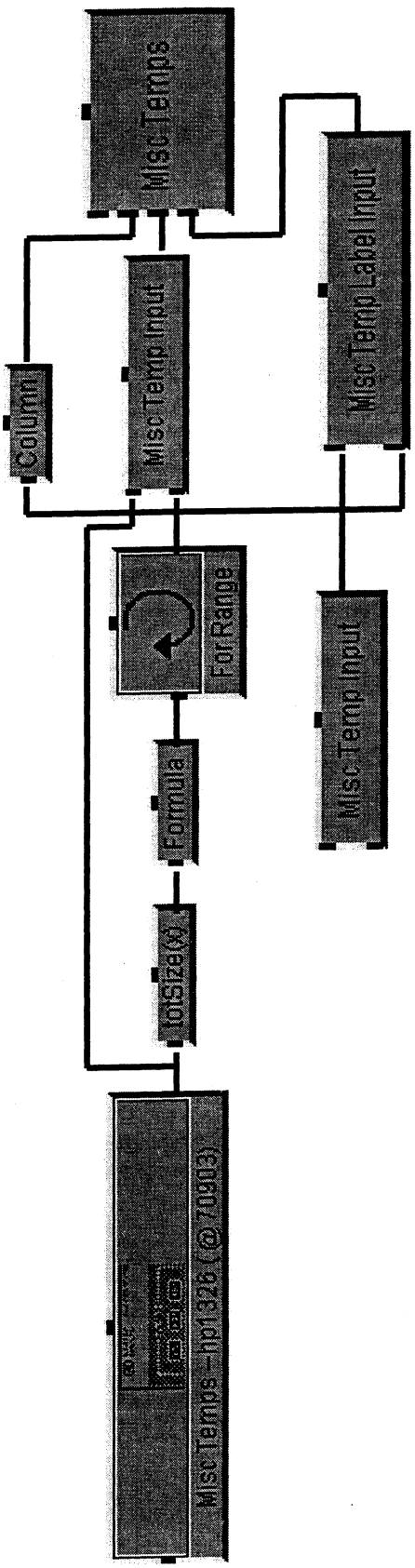

Figure C.1. Sample HP VEE Subroutine

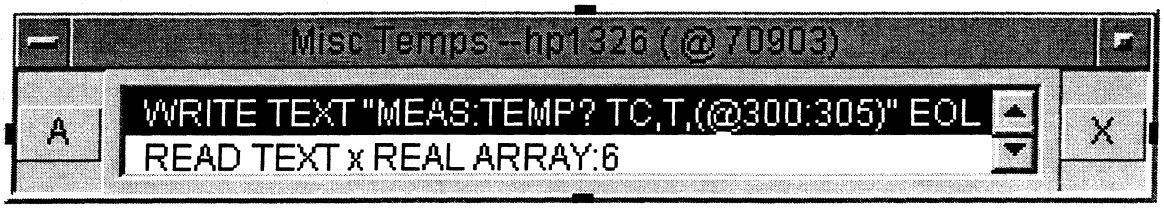

Figure C.2. "Misc Temp – hp1326 (@70903)" Box for Temperature Measurements

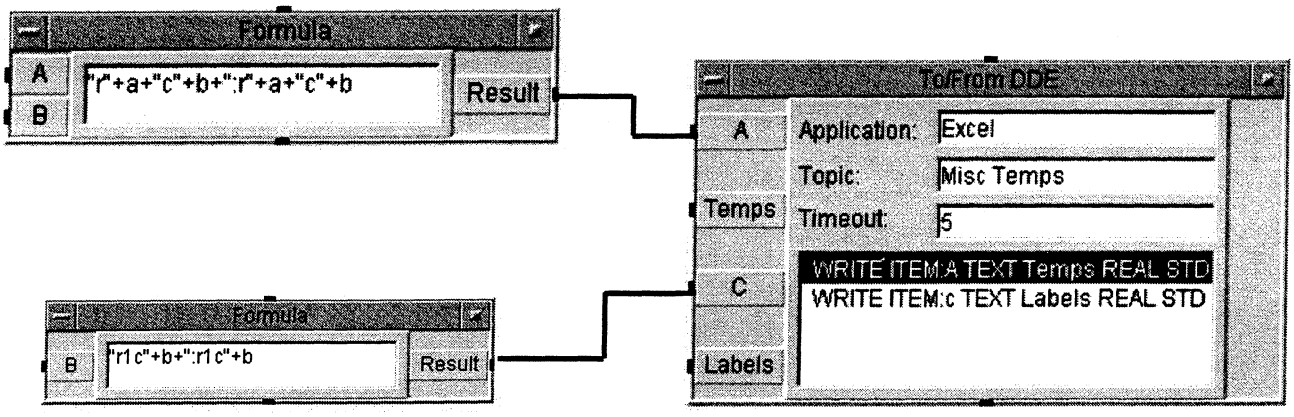

Figure C.3. "Misc Temp" Box for Export to Excel

Appendix D

Enthalpy at the Exit of the Compressor

This section contains information on the development of curves fits for an accurate estimation of enthalpy at the superheated conditions in the vapor line just prior to the mixing point. An EES code for the determination of the pressure and enthalpy values in superheat is included as well as some of the plots formulated to obtain the curve fits. These fits are for R134a and R410A.

D.1. EES Code for Superheated Pressure-Enthalpy Values

{This program generates data for the Enthalpy-Pressure Plots. These plots were used in order to calculate the vapor enthalpy prior to mixing.}

{Saturated Inlet Range}
P_low=pressure(R134a,T=-10,x=.5)
P_mid1=pressure(R134a,T=-5,x=.5)
P_mid2=pressure(R134a,T=0,x=.5)
P_mid3=pressure(R134a,T=15,x=.5)
P_mid4=pressure(R134a,T=25,x=.5)
P_mid5=pressure(R134a,T=35,x=.5)
P_high=pressure(R134a,T=50,x=.5)

{Superheat Compressor Region for T=0 to 50 deg C}

{Low Compressor Exit Temps}
n1=6
Duplicate i=1,n1
T_super_low[i]=lookup(i,1)
h_low[i]=enthalpy(R134a,P=P_low,T=T_super_low[i])
End

{Mid 1 Compressor Exit Temps}
n2=6
Duplicate i=1,n2
T_super_mid1[i]=lookup(i,2)
h_mid1[i]=enthalpy(R134a,P=P_mid1,T=T_super_mid1[i])
End

```
{Mid 2 Compressor Exit Temps}
n3=6
Duplicate i=1,n3
T_super_mid2[i]=lookup(i,3)
h_mid2[i]=enthalpy(R134a,P=P_mid2,T=T_super_mid2[i])
End

{Mid 3 Compressor Exit Temps}
n4=4
Duplicate i=1,n4
T_super_mid3[i]=lookup(i,4)
h_mid3[i]=enthalpy(R134a,P=P_mid3,T=T_super_mid3[i])
End

{Mid 4 Compressor Exit Temps}
n5=3
Duplicate i=1,n5
T_super_mid4[i]=lookup(i,5)
h_mid4[i]=enthalpy(R134a,P=P_mid4,T=T_super_mid4[i])
End

{Mid 5 Compressor Exit Temps}
n6=2
Duplicate i=1,n6
T_super_mid5[i]=lookup(i,6)
h_mid5[i]=enthalpy(R134a,P=P_mid5,T=T_super_mid5[i])
End

{High Compressor Exit Temps}
n7=1
Duplicate i=1,n7
T_super_high[i]=lookup(i,7)
h_high[i]=enthalpy(R134a,P=P_high,T=T_super_high[i])
End
```

D.2. Curve Fit Plots

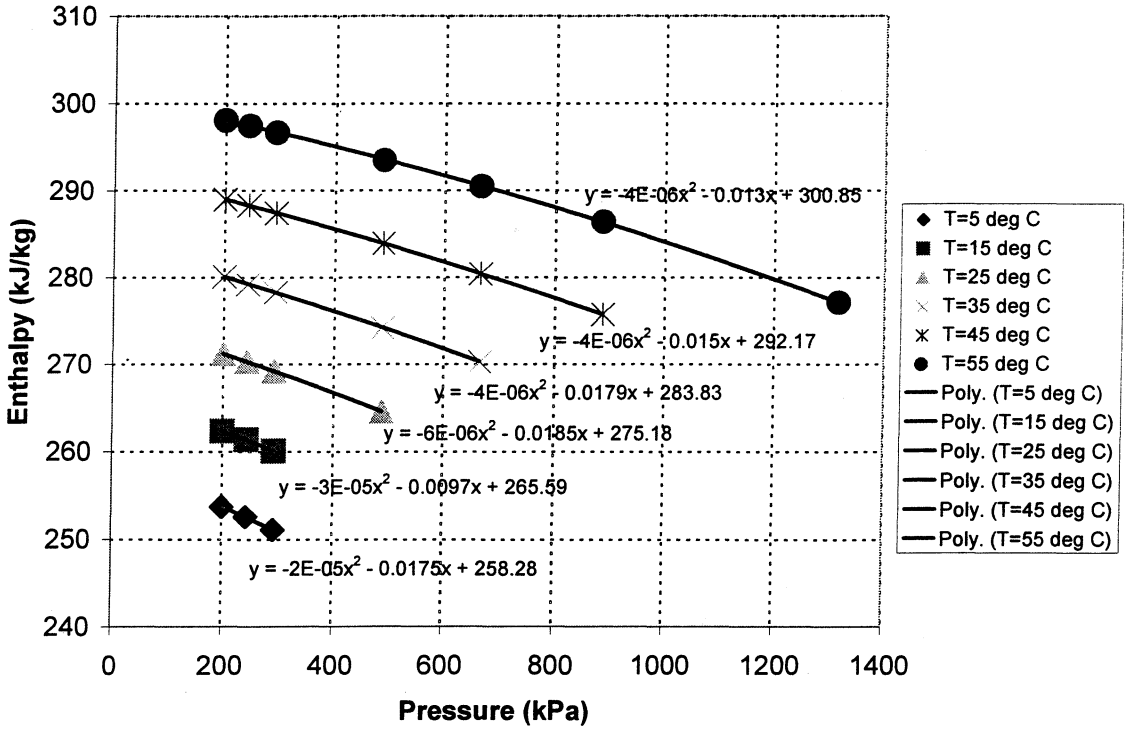

Figure D.1. Enthalpy vs. Pressure for R134a

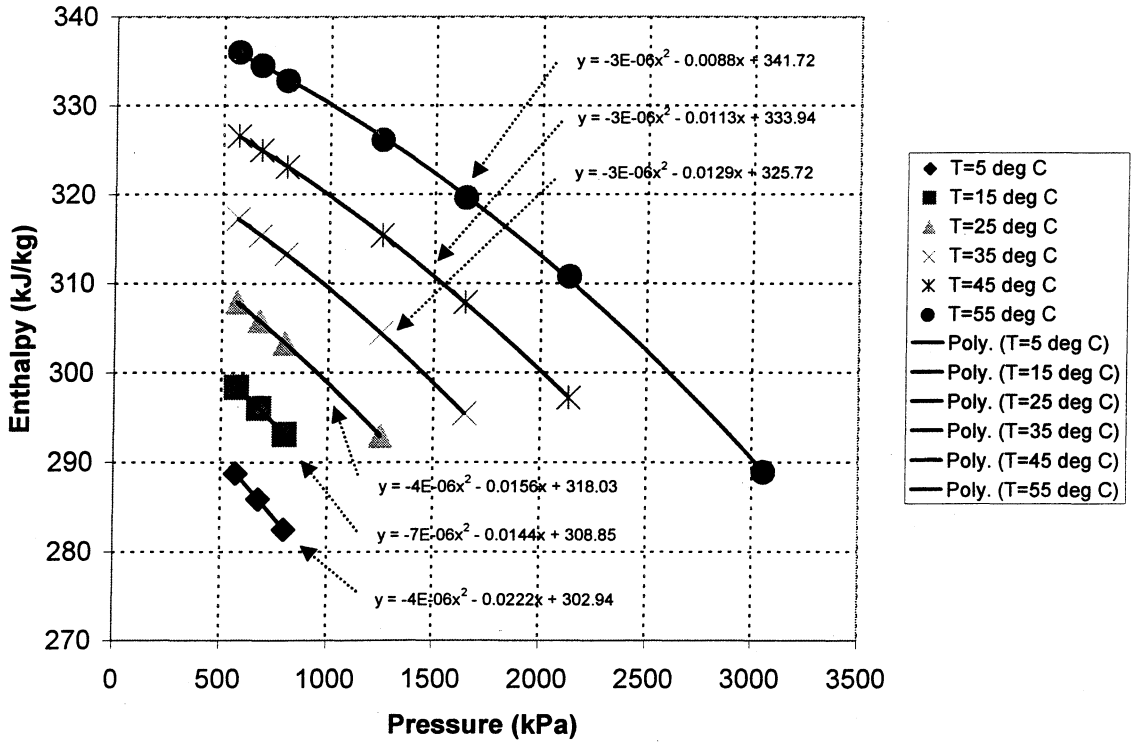

Figure D.2. Enthalpy vs. Pressure for R410A

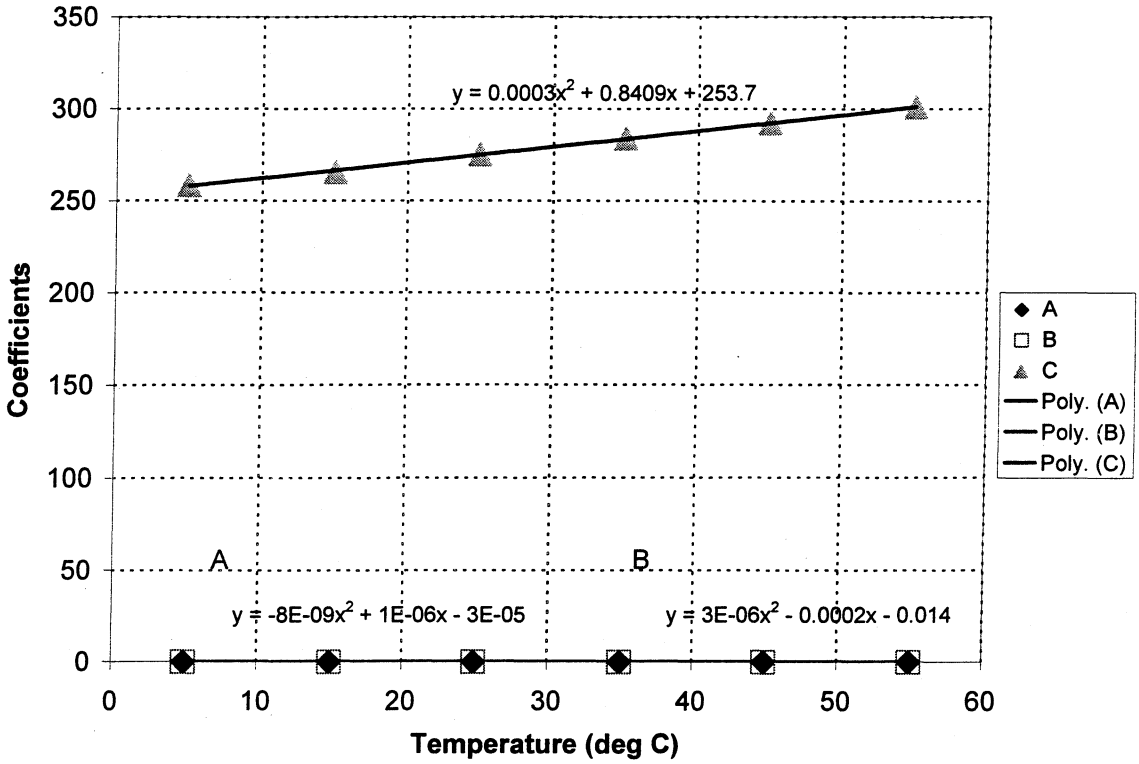

Figure D.3. Enthalpy Coefficients vs. Temperature for R134a

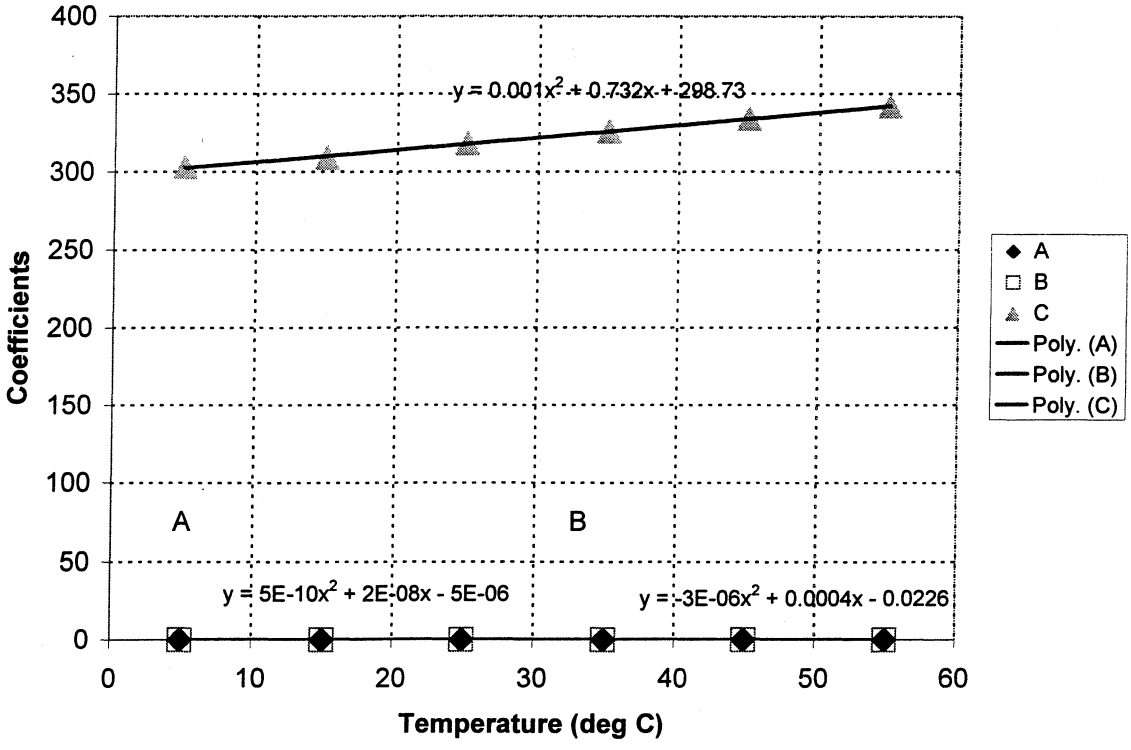

Figure D.4. Enthalpy Coefficients vs. Temperature for R410A

Appendix E

EES New Apparatus Condition Code

The following EES program will give approximate mass flow rates for the desired quality and mass flux conditions.

{Input the following values. The pressure and temperatures should be approximate values obtained from HP VEE. The x_m is the test section inlet quality desired and the mflux is the mass flux desired. A is the cross sectional area of the test section. It is used in calculating mass flux. }

```
P_phin=320        {kPa}
T_phout=3         {deg C}
P_comp=320        {kPa}
T_comp=15         {deg C}

x_m=.5            {Quality -- in fraction form}
mflux=500         {kg/m^2 s}
A=51.08*10^(-6)   {m^2}


{Liquid Line}
T_l=T_phout
P_l=P_phin
v_l=volume(R134a,T=T_l,x=0)
P_l_sat=pressure(R134a,T=T_l,x=0)
dp_l=P_phin-P_l_sat
h_l=enthalpy(R134a,T=T_l,x=0)-v_l*dp_l


{Vapor Line}
T_v=T_comp
P_v=P_comp
v_v=volume(R134a,T=T_v,x=1)
P_v_sat=pressure(R134a,T=T_v,x=1)
dp_v=P_comp-P_v_sat
h_v=enthalpy(R134a,T=T_v,x=1)+v_v*dp_v
```

{Final/Mixed Conditions}
T_sat=5
T_m=T_sat
P_m=pressure(R134a,T=T_m, x=.5)
mdot_m=mdot_v+mdot_l
h_m=(mdot_v*h_v+mdot_l*h_l)/mdot_m
h_sat_l=enthalpy(R134a,T=T_sat,x=0)
h_sat_v=enthalpy(R134a,T=T_sat,x=1)

x_m=(h_m-h_sat_l)/(h_sat_v-h_sat_l)

mflux=mdot_m/A